NASA CR-137772

Transient Airload Computer Analysis For Simulating Wind Induced Impulsive Noise Conditions of a Hovering Helicopter Rotor

By Gerald F. Hall

October, 1975

Prepared under Contract No. NAS2-7025 by
UNITED TECHNOLOGIES RESEARCH CENTER
East Hartford, Connecticut

for

U.S. ARMY AIR MOBILITY RESEARCH AND DEVELOPMENT LABORATORY

AMES DIRECTORATE

TRANSIENT AIRLOAD COMPUTER ANALYSIS FOR SIMULATING WIND INDUCED IMPULSIVE NOISE CONDITIONS OF A HOVERING HELICOPTER ROTOR

Gerald F. Hall
United Technologies Research Center

SUMMARY

A numerical analysis was developed to determine the airloads of helicopter rotors operating under near-hovering flight conditions capable of producing impulsive noise. The development of the transient wake and airload analysis has resulted in a computer program in which the solution for the hovering rotor tip vortex geometry, inflow, aeroelastic response and airloads are solved in a coupled manner at sequential time steps, with or without the influence of an imposed steady ambient wind or transient gust. The computer program was developed for future applications in which predicted airloads would be incorporated in an acoustics analysis to attempt to predict and analyze impulsive noise (blade slap).

The computer analysis was applied to a hovering full-scale rotor for which impulsive noise was recorded in the presence of ambient wind. Although blade airloads data were not available for this rotor, the results from the initial applications of the computer analysis, as applied to this rotor operating with and without a steady ambient wind, are somewhat encouraging. The predicted tip vortex coordinates are in reasonable agreement with the limited test data, and the blade airload solutions converged to a periodic behavior for an imposed steady ambient wind condition. However, the requirement for refinements to the analysis is evident, particularly for impulsive noise applications where high harmonics of blade airloading are required. Recommended refinements and suggestions for continued evaluation of the analysis are presented.

INTRODUCTION

The impulsive noise due to blade-vortex interaction, commonly known as blade slap, is a dominant source of helicopter rotor noise. An understanding of its mechanism of generation and a method for predicting it are necessary if a reduction in aircraft annoyance and detection are to be achieved. The commercial and military applications of the helicopter dictate as quiet a machine as possible, yet certain operating regimes give rise to impulsive noise levels high enough to jeopardize a military mission or be uncomfortable to commercial passengers.

Various investigations have indicated that blade slap arises from the unsteady lift fluctuation on a blade due to the induced flow field caused by the tip vortex of another blade. An investigation into the noise generation of a full-scale hovering rotor subjected to low-speed wind conditions is reported in Ref. 1. The results of this test program indicate that blade slap depends on blade-vortex interaction and compressible conditions at the tip. All the test conditions of Ref. 1 had blade-vortex intersections or near intersections and yet did not necessarily produce impulsive noise. It was subsequently found (Ref. 2) that the impulsive noise boundary coincided very closely to conditions beyond which local blade sonic velocities occurred. It was concluded that the impulsive noise due to blade vortex interaction of a single hovering rotor required a moving vortex to pass close enough to the tip to either drive the tip locally supersonic for a short duration giving rise to a rapidly forming and disappearing shock wave or to cause a fluctuating motion to an already existing shock wave. In Ref. 2, it is postulated from the whirl tower test results of Ref. 1 that the criteria for rotor impulsive noise are: (1) the vortex from a preceding blade must pass near the blade producing noise, and (2) a shock wave must exist (or nearly exist) on the surface of the blade where the vortex passes. Thus, the accurate prediction of impulsive noise requires an ability to accurately predict the following:

1. the tip vortex position relative to the blade,

2. the flow velocities at the blade including those induced by the rotor wake (particularly the velocities induced by the near tip vortex), and

3. the associated blade airloads including compressibility effects.

Whereas rotational noise can be predicted by existing methods, impulsive noise prediction is difficult at best. The sensitivity of the induced velocity field in hover to the tip vortex position is well known (Ref. 3). Fluctuations

in this velocity field due to variations in the tip vortex position will cause existing shock waves to fluctuate or cause local sonic regions to alternately form and collapse. Both situations give rise to a fluctuating pressure field which can create unacceptable noise levels. Since the sound pressure level is directly dependent on both the instantaneous force and its timewise rate of change, it is apparent that a requirement exists for an accurate prediction of the time history of rotor airloads in order to produce impulsive noise.

Vortex induced blade slap has occurred in hover and low speed conditions where the tip vortices pass close to the blades producing a major increment to the total velocity and airloading at the blades. Several analyses have been developed by Landgrebe at the United Technologies Research Center (UTRC) for computing the aerodynamic interactions between helicopter rotor blades and the rotor wake for the determination of blade airloads and response characteristics (e.g., Refs. 3 through 5). A UTRC method for the hover condition is reported in Refs. 3 and 4. This method assumes the hover condition to be steady, with the tip vortex pattern from each blade similar and constant with time producing steady airloads. It has been hypothesized for hover that a small amount of ambient wind is required to produce the unsteady airloading required for impulsive noise. The ambient wind may itself be unsteady (a transient gust) which results not only in an unsteady variation of the wake geometry and airloads but also in a nonperiodic variation requiring a transient solution. Techniques used in the above references, were thus applied and extended to develop a new analysis applicable to transient conditions. Some techniques developed by the author in Ref. 6 were also applied. The analysis considers the rotor to be operating initially in a hover mode and then, as the gust is applied, the wake is allowed to convect under both the gust and its own self induced velocities. The blade inflow velocities and the time histories of the blade loadings are then determined. A simplified aeroelastic analysis to determine the first flatwise bending mode contribution is included.

The objectives of this research program were to:

1. extend the applicability of the existing methods to predict rotor wake geometry, inflow, and airloads for hovering rotors operating under conditions producing impulsive noise,

2. provide the Government with the computer program developed so that airloads could be predicted and incorporated in a Government acoustics analysis to study the impulsive noise phenomena, and

3. demonstrate and perform an initial assessment of the analysis.

This report contains a description of the computer analysis developed and results from initial applications which were performed to demonstrate and obtain an initial assessment of the analysis. Results for a hover condition without ambient wind are followed by results for the same condition with ambient wind, for which blade slap was encountered as reported in Ref. 1.

LIST OF SYMBOLS

a_o	Section lift curve slope
A_{ls}, B_{ls}	Longitudinal and lateral cyclic pitch control, respectively, deg
c	Blade chord, m
c_e	Section lift coefficient
C_{N_i}, $C_{N_i'i'}$	Constants defined in Ref. 7 which are integral functions of the blade mass distribution, chordwise center of gravity, and flatwise mode shapes and their derivatives.
e	Flapping hinge offset, m
g	Gravity, m/sec^2
m	Blade mass per unit span, $\frac{n\text{-}sec^2}{m^2}$
q_w	Flapwise modal deflection
$\vec{r}$	Radius vector from vortex filament to point, P, where induced velocity is determined
r_g	Radius of gust front from center of rotor, m
R	Blade radius, m
$d\vec{s}$	Differential length of vortex filament
$(S_A)_z$, $(S_A)_y$	Normal and inplane blade loads, respectively, n
t	Time, sec.
U	Resultant velocity at radial station, m/sec
U_p	Velocity at radial station normal to tip path plane, m/sec
U_T	Velocity at radial station parallel to tip path plane, m/sec
$\vec{V}$	Velocity, m/sec

$\vec{v}_{i_p}$	Induced velocity at point, P, m/sec
$\vec{v}_g$	Gust velocity, m/sec
w_e	Flapwise deflection
x, y, z	Cartesian coordinate system components
α, β	Included angles between ends of straight line vortex segment and point at which induced velocity is calculated
α	Also, blade section angle of attack, deg
α_s	Rotor shaft angle of attack, deg
β	Also, blade f[illegible]ng angle
γ_w	Flapwise mode [illegible]e
Γ	Circulation, m^2/sec
λ_s	Inflow ratio (see Eq. 19)
μ	Rotor advance ratio
θ_1	Blade linear twist angle, deg
θ_o	Collective pitch, deg
θ_g	Inclination angle of normal to gust front, deg
ψ	Blade azimuth angle, deg
ω	Natural frequency of i^{th} flatwise mode, rad./sec., also frequency of transient gust
Ω	Propeller rotational speed, rad./sec.

Subscripts

5	Rigid blade axis system at a blade section (Ref. 7)
10	Final deformed axis system at a blade section, including bending translation and rotation and twist (Ref. 7)
i, i'	Flapwise mode shape indices
c.g.	Distance of center of gravity from elastic axis
3c/4	Distance of three quarter chord from elastic axis
w	Flapwise mode

Miscellaneous Notations

$( )'$	Derivative with respect to $\bar{r}$
$(^{*})$	Derivative with respect to ψ (time)

THEORETICAL DEVELOPMENT

Numerical Model

The prediction of airloads and wake geometries of a rotor under the action of a transient gust represents one of the most formidable of aerodynamic problems. Since such a gust is usually of short duration and can be time dependent, determination of the ensuing loading and vortex wake motion is an inherently unsteady aerodynamic problem. The fact that the gust convects the vortex wake, the motion of which affects the loading continuously in time, specifies the problem to be one in unsteady aerodynamics.

In order to model the problem of the rotor and its wake interaction with the gust, certain assumptions are made. The basic assumption is that the rotor and its wake operate in an inviscid medium, and the disturbance they create is irrotational; i.e., the problem is a potential flow problem. The blades can be assumed to be represented by concentrated bound vortices which amounts to neglecting the details of chordwise loading. This is the standard lifting line assumption. The wake behind the blades is a surface containing a distribution of vorticity. This distributed vorticity can be subdivided into two parts: 1) the trailing vorticity which is aligned more or less with the local velocity, satisfies the Helmholz vortex continuity criterion at the blades and provides pressure equalization at the tips; 2) shed vorticity which is laid down initially parallel to the trailing edge and is determined by the timewise variations in bound circulation so as to satisfy the Kutta condition at the trailing edge. Although shed vorticity can potentially be of significance in the determination of the timewise variation of blade loading, as will be discussed, accurate vortex modeling of its effect at the blade without exceeding practical computer limitations remains to be developed. Shed vorticity was thus neglected at this stage of the development of the analysis.

The loading at the blades is strongly dependent on the induced velocity field of the vortex wake which, in turn, depends on its instantaneous position. The instantaneous position of a wake point depends on the time history of the velocity field under which it was convected from the instant it was deposited in the wake until the current time. This velocity field can consist of a variety of imposed motions (flight speed, gust, blade rotation, etc.) as well as its own self-induced velocity field. While many flight conditions permit neglect of wake self-induced velocities as compared to some larger imposed motion, in the hover or near-hover case wake-induced velocities are a primary source of transport and cannot be neglected. Thus, a nonlinear flow

problem is defined which precludes any hope of closed form solution, and numerical methods are therefore employed. Figure 1 is a computerized representation of the wake beneath a hovering rotor from Ref. 3. The aerodynamic complexity is evident from the complexity of this wake geometry.

The numerical treatment considered uses vortex techniques in which the continuous vorticity distribution in the wake is approximated by several trailing vortex filaments divided into straight segments. The blade bound vortices are broken up into a discrete number of radial segments over which the loading of each is assumed constant.

In the physical process of a finite lifting surface moving through a fluid, trailing vorticity, with strength equal to the spanwise bound circulation gradient at the instant of shedding, is continuously deposited in the wake. The numerical counterpart, which analyzes the lifting surface at discrete time intervals, lays down trailing vortices with initial lengths defined by the distance the surface travels during a time interval. Its strength is the bound circulation gradient at the beginning of a time interval. The possible difference in trailer strengths that occur because of time variable loading is taken up by the shed vorticity (neglected in this analysis) deposited at the beginning of each time interval. To magnify the complexity of the problem, the individual wake points see different velocity fields (any time or spatially variant imposed motion as well as self-induced), and so can move different distances during a given time interval. The vortex segments are free to deform, stretch, and rotate.

Under the basic assumptions just stated, a model for the rotor wake system under the transient gust can be formulated. Initially, the rotor and its wake are assumed to exist in some "steady state" condition. At some instant, a gust velocity, which can have components in the rotor plane and normal to it, begins to move across the rotor wake system (in the general case as a wave front). Points in the wake are then transported by the gust velocity, as well as their own self-induced field, as they enter the gust. Also, the blade itself may enter and leave the gust, depending on the speed of the gust front. These continuously occurring phenomena lead to an unsteady aperiodic loading on the rotor blades.

A numerical approximation to the above described model does not treat the continuously varying problem, but rather yields a solution only at discrete time intervals. As a result, the following numerical model is used to approximately describe the continuous physical process. The rotor and its wake are initially assumed to exist in an initial "steady state" condition. That is, an initial circulation distribution, induced velocity distribution, and wake geometry are specified. Then, at some instant of time,

t, the gust is assumed to begin moving across the rotor-wake system. Wake points are assumed to be convected with the induced velocity the points incur at time, t, as well as the gust velocity if the points lie behind the gust front. This transport velocity is assumed constant over the small time increment, Δt. Hence, the wake points move the incremental distance, $\vec{V}\,\Delta t$, where $\vec{V}$ is the sum of all imposed velocities including the gust and the self-induced velocities. During the same time interval the blades are allowed to advance a rotation distance $\Delta\psi = \Omega\Delta t$, where $\Delta\psi$ is an azimuth angle increment and Ω is the rotational speed. Trailing vorticity is deposited from the blades along the path of travel. At the end of the time interval, Δt, a new inflow at the blades and accompanying circulation distribution and loading is determined. The process is repeated for as many time steps as deemed necessary to describe the solution to the problem. Figure 2 shows a representative comparison between the continuous wake model comprised of a continuous sheet of vorticity and the segmented wake required for computational analysis.

Wake Convection

The wake points are convected under the action of their self-induced velocity field, the blade-induced velocity and the gust velocity.

Wake self-induced velocity and blade-induced velocity. - The self-induced velocity field of the vortex wake and the blade-induced velocity field are determined by repeated application of the Biot-Savart law,

$$d\vec{v}_{i_p} = \frac{\Gamma}{4\pi}\,\frac{\vec{r}\times d\vec{s}}{|\vec{r}|^3} \tag{1}$$

where dv_{i_p} is the differential velocity induced at a point in space, P, by the vortex segment of strength, Γ, and differential length, ds, located a distance r from the vortex segment. Figure 3 shows this geometry. From Ref. 3, for a straight line vortex segment of finite length, the induced velocity can be expressed in Cartesian component form as follows:

$$v_{x_p} = \frac{\Gamma}{4\pi}\,\bar{K}\left[(\bar{y}_p-\bar{y}_A)\,(\bar{z}_p-\bar{z}_B) - (\bar{y}_p-\bar{y}_B)\,(\bar{z}_p-\bar{z}_A)\right]$$

$$v_{y_p} = \frac{\Gamma}{4\pi}\,\bar{K}\left[(\bar{z}_p-\bar{z}_A)\,(\bar{x}_p-\bar{x}_A) - (\bar{z}_p-\bar{z}_B)\,(\bar{x}_p-\bar{x}_B)\right]$$

$$v_{z_p} = \frac{\Gamma}{4\pi}\,\bar{K}\left[(\bar{x}_p-\bar{x}_n)\,(\bar{y}_p-\bar{y}_B) - (\bar{x}_p-\bar{x}_B)\,(\bar{y}_p-\bar{y}_A)\right]$$

$$\bar{K} = \frac{1}{R} \frac{(AP + BP)/(AP)(BP)}{(AP)(BP) + I + J + K}$$

$$I = (\bar{x}_p - \bar{x}_A)(\bar{x}_p - \bar{x}_B) \qquad (2)$$

$$J = (\bar{y}_p - \bar{y}_A)(\bar{y}_p - \bar{y}_B)$$

$$K = (\bar{z}_p - \bar{z}_A)(\bar{z}_p - \bar{z}_B)$$

$$AP = \left[(\bar{x}_p - \bar{x}_A)^2 + (\bar{y}_p - \bar{y}_A)^2 + (\bar{z}_p - \bar{z}_A)^2\right]^{1/2}$$

$$BP = \left[(\bar{x}_p - \bar{x}_B)^2 + (\bar{y}_p - \bar{y}_B)^2 + (\bar{z}_p - \bar{z}_B)^2\right]^{1/2}$$

Inherent in the use of straight line vortex segments for modeling the curved vortex wake are the problems of 1) accounting for the curvature of the segments and 2) the fact that a singularity in the Biot-Savart law exists when the point at which the induced velocity is calculated lies on the inducing element.

The error due to neglect of vortex curvature increases as the point at which the induced velocity is determined gets close to the inducing filament. In the vortex wake the points at which the induced velocity is calculated are endpoints of the inducing vortex segments. Thus a relatively large error can be expected at these points due to neglect of curvature. In an attempt to account for this effect the approach developed for the Vortex Geometry Analysis in Ref. 3 is used. Here it is assumed that the segments adjacent to the point in question can be approximated by circular arcs and their effects can be obtained by scaling the influence of adjacent straight segments according to the equation:

$$v_i = v_{i_o} + 2K v_{i_A} \qquad (3)$$

where v_i = Induced velocity at point, P.

v_{i_o} = Induced velocity at P, based on straight segments.

v_{iA} = Velocity induced by the wake segment that adjoins the wake segment adjacent to the wake point. P.

K = Scaling factor for curvature, a function of vortex core radius and azimuth increment (straight line segment length).

The value of K, included as input in the numerical analysis, is given in Fig. 4.

The singularity in the Biot-Savart law is eliminated by assuming the vortex segment to really have a small but finite core inside of which potential flow considerations do not apply. Recognizing the complexity of the real flow inside such a region to be beyond the scope of the exterior potential flow model, it is assumed simply that each filament segment in the wake conserves circulation per unit length and maintains a solid body rotation within the core region. Hence, within the core

$$\vec{v}(\vec{r}) = \vec{v}_1(\vec{r})\left(\frac{r}{r_c}\right)^2 \frac{\cos\alpha_c + \cos\beta_c}{\cos\alpha + \cos\beta} \tag{4}$$

where $v_1(r)$ = Velocity induced at $r < r_c$ by Biot-Savart law

r_c = Core radius

$\alpha, \beta, \alpha_c, \beta_c$ = Vortex segment geometry, Fig. 5

The vortex core radius must be input in the analysis.

Finally, it must be stated that the wake induced velocity is computed in an inertial coordinate system shown in Fig. 6. This coordinate system identifies the $\psi = 0°$ (zero azimuth) position of the blades and also serves as a reference system for the gust velocity.

Gust representations. - Various representations for the transient gust are considered. The positive convention for all the models is shown in Fig. 7. The least complex gust is a simple step change in the velocity imposed on all the rotor and wake points at some initial instant of time and held constant in magnitude and direction for all time.

$$\vec{v}_g = \begin{cases} 0 & t < t_o \\ \vec{i}\, v_{g_x} + \vec{j}\, v_{g_y} + \vec{k}\, v_{g_z} & t < t_o \end{cases}$$

$$\tan\theta_g = v_{g_y}/v_{g_x} \tag{5}$$

where θ_g is the angular orientation of the gust in-plane velocity relative to the inertial reference. This particular gust representation has as an analogy in fixed-wing aerodynamics as the classic Wagner gust representation.

A more complex model consists of the gust moving across the rotor wake system as a traveling wave so that a finite time must elapse before the entire system is immersed in the gust. Hence, a point may or may not be affected by the gust accordingly as it is behind or ahead of the gust front. Of this model, two possibilities are considered. One has a completely uniform velocity field behind the gust front so that

$$\vec{v}_g(t) = \begin{cases} 0 \text{ before gust passage} \\ \vec{i}v_{g_x} + \vec{j}v_{g_y} + \vec{k}v_{g_z}, \text{ after gust passage} \end{cases} \tag{6}$$

and v_{gx}, v_{gy}, v_{gz} are all constant. This situation is shown in Fig. 7. To determine whether or not a point lies behind the gust front, let the radius vector normal to the front at any instant of time be given by

where
$$\vec{r}_g(t) = \vec{r}_g(0) + V_g t$$
$$\vec{V}_g = \vec{i}\,v_{g_x} + \vec{j}\,v_{g_y} \tag{7}$$
$$\vec{r}_g(0) = \vec{r}_g \text{ at the initial time}$$

Referring to Fig. 7, the collection of points lying on the gust front satisfies the relation

$$\frac{x_g - r_g \cos\theta g}{y_g - r_g \sin\theta g} = -\tan\theta g \tag{8}$$

Then, if $(x_p,y_p) < (x_g,y_g)$ the point (x_p,y_p,z) lies behind the gust front and the point is thus influenced by the gust velocity

$$\vec{v}_g = \vec{V}_g + \vec{k}\,v_{gz} \quad V_g \tag{9}$$

where $\vec{V}_g$ = In plane gust velocity, a constant

$\vec{v}_{gz}$ = Normal gust velocity, a constant

Another degree of complexity to the traveling wave gust can be added by assuming a time dependent normal gust velocity of sinusoidal form

$$v_{gz} = b \sin \omega t_1 \tag{10}$$

where b is a velocity amplitude, ω a given frequency, and t_1 a "retarded time" which measures the time since the gust front passed the point (x_p, y_p, z_p). Hence the gust velocity is represented by

$$\vec{V}_g = \begin{cases} 0 & (x_p, y_p) > (x_g, y_g) \\ \vec{V}_g + \vec{k}\, b \sin \omega t_1 & (x_p, y_p) < (x_g, y_g) \end{cases} \tag{11}$$

where (x_p, y_p) are the in-plane Cartesian coordinates of the point in question and (x_g, y_g) are the in-plane coordinates of points on the gust front. The time, t_1, that the point has spent in the gust, relative to the gust front location is

$$t_1 = \frac{|\vec{r}_g| - |\vec{r}_p| \cos(\theta_p - \theta_g)}{|\vec{V}_g|} \tag{12}$$

Thus, a point, (x_p, y_p, z_p) is determined to be behind or ahead of the gust front, and its velocity is then determined by the position relative to the gust front, as determined by t_1.

If desired, the analysis could easily be expanded to include other types of gusts such as a ramp gust in which the velocity normal to the tip path plane increases linearly with position in the gust. Hence, the gust velocity would be given by

$$\vec{V}_g = \begin{cases} 0 & (x_p, y_p) > (x_g, y_g) \\ \vec{V}_g + \vec{k}\, m \left[\dfrac{|\vec{r}_g| - |\vec{r}_p| \cos(\theta_p - \theta_g)}{\vec{V}_g} \right] & (x_p, y_p) < (x_g, y_g) \end{cases} \tag{13}$$

where m is the gust acceleration in the direction normal to the tip path plane.

Thus, in accordance with the gust model desired, wake points convect under the gust velocity as well as their own self-induced velocities.

Determination of Circulation and Inflow

In order to determine the wake induced velocity field at any instant of time, the wake circulation distribution must be known. To determine the circulation within the framework of lifting line theory, the fundamental circulation equation (Eq. 14) is used. This equation is an implicit statement of the Weissinger lifting surface theory boundary condition.

$$\Gamma(r,\psi) = \frac{U(r,\psi)}{2} c(r)\, c_{\ell}(r,\psi) = \frac{U(r,\psi)}{2} c(r) a_o(r,\psi) \alpha(r,\psi) \tag{14}$$

and

$$U(r,\psi) = \left[U_T^2(r,\psi) + U_p^2(r,\psi)\right]^{1/2} \tag{15}$$

where $U(r,\psi)$ is the resultant velocity at the radial station, r, of a blade located at azimuth location ψ; c is the local chord; a_o is the lift curve slope of the section; α is the local angle of attack. $\Gamma(r,\psi)$ is the local bound circulation at the "r" radial position on the blade at azimuth angle ψ. The circulation is stall limited with a maximum value determined from the section steady state stall. The angle of attack (Fig. 8) contains the blade pitch angle, any cyclic angles, aeroelastic motion and induced velocities, due to both the wake and other blades. As a result

$$\alpha(r,\psi) = \Theta + \tan^{-1} U_p/U_T \tag{16}$$

where

$$\frac{U_p}{\Omega R} = \lambda_s\left(1 - \frac{\beta^2}{2}\right) - \mu\beta\cos\psi - \frac{*}{w_e}\cos\theta + \overline{w}_e\,\theta^*\sin\theta$$

$$-\overline{y}_{10_{\frac{3c}{4}}}\theta^*\cos\theta - \beta'\left(\overline{y}_{10_{\frac{3c}{4}}}\cos\theta - \overline{w}_e\sin\theta\right) - r\beta^* \tag{17}$$

$$+\overline{w}_e'\cos\theta\left(-\mu\cos\psi - \lambda_s\beta - \overline{y}_{10_{\frac{3c}{4}}}\right) - \theta'\mu\cos\psi\,\overline{w}_e\sin\theta$$

$$\frac{U_T}{\Omega R} = \mu \sin\psi + \bar{e} + \bar{r}\left(1 - \frac{\beta^2}{2}\right) + \bar{y}_{IO_{\frac{3c}{4}}}\overset{*}{\theta} \sin\theta - \overset{*}{\bar{w}_e} \sin\theta$$

$$- \bar{w}_e \overset{*}{\theta} \cos\theta - \beta\left(\bar{w}_e \cos\theta + \bar{y}_{IO_{\frac{3c}{4}}} \sin\theta\right) + \bar{w}_e' \sin\theta\left(-\mu\cos\psi\right. \tag{18}$$

$$\left. - \lambda_s\beta - \bar{y}_{IO_{\frac{3c}{4}}} \cos\theta\right) - \theta' \bar{w}_e \cos\theta\, \mu\cos\psi$$

and

$$\lambda_s = \frac{V\sin\alpha_s - v_{iz}}{\Omega R} \tag{19}$$

Equations 17 and 18 are developed fully in the aeroelastic analysis of Ref. 7 where they include flatwise, edgewise and torsion effects. Here they have been modified to include only flapping and flatwise bending, and lead-lag effects have been neglected. Equation 17 was modified to include the vertical gust component

$$\frac{U_p}{\Omega R} = \text{Equation 17} + \frac{v_{gz}}{\Omega R} \tag{20}$$

Even though the in-plane gust component should be small relative to the rotational velocities, and so could be neglected without serious effects in $U_T/\Omega R$, it was also included. Thus

$$\frac{U_T}{\Omega R} = \text{Equation 18} + \frac{v_{gx}\sin\psi - v_{gy}\cos\psi}{\Omega R} \tag{21}$$

The angle, Θ, includes blade collective pitch, twist and control system input so that

$$\Theta = \theta_0 + \theta_B \tag{22}$$

$$\theta_B = \theta_1(\bar{e} + \bar{r} - 0.75) \tag{23}$$

$$\theta_0 = \theta_{75R} - A_{1S}\cos\psi - B_{1S}\sin\psi \tag{24}$$

where $\theta_{.75}$ is the collective pitch at 0.75 radius, θ_1 is the linear twist over the radius, and A_{1s} and B_{1s} are control inputs. Pitch-flap coupling effects are neglected. The quantity, λ_s, is the inflow ratio and contains the induced aerodynamics. As a result it contains induced velocity contributions from all bound and wake vortex elements. Equation 14 can be written for a number of radial stations on each blade. The aerodynamics of the blade and wake system enters through the section angle of attack, α, which contains the induced velocity of the wake as well as the effect of other blades. The system of equations developed by applying Eq. 14 in this manner can be expressed as a set of simultaneous equations with the unknown bound circulations, Γ_j's, at the various radial stations to be determined.

$$A_{ij} \Gamma_j = B_i \tag{25}$$

Here the subscript i identifies the particular load point at which the velocity is induced, j identifies an inducing element of unknown strength, Γ_j. A_{ij} is the influence coefficient which incorporates the effect of relative geometry between the j^{th} unknown vortex segment and the i^{th} load point. B_i represents the known inflow at the i^{th} load point and includes all known velocities normal to the tip path plane. This is a fairly standard approach and has been used with success for a number of years (e.g., Refs. 3 - 5).

Blade Loads and Aeroelastic Effects

The aeroelastic effects are developed in detail in Ref. 7. The pertinent equations and the implementation in the computer program are discussed here. A major assumption in accounting for the aeroelastic effects is that flatwise motions and deflections are the major contribution for the hover conditions so that edgewise and torsion characteristics can be neglected. Hence the equations of flatwise bending for a given blade as given in Ref. 7 are reproduced here, neglecting the edgewise and torsion effects.

$$0 = \int^{\bar{r}_T} \gamma_{w_i} \left[(\bar{S}_A)_{z_5} \cos \Theta - (\bar{S}_A)_{y_5} \sin \Theta \right] d\bar{r} - C_{1_i} \left\{ \ddot{q}^{**}_{w_i} + q_{w_i} \left[\bar{\omega}_{w_i}^2 \right.\right.$$

$$\left. - \dot{\theta}_0^{*2} - 2\beta \dot{\theta}_0^{*} + \beta \sin 2\theta_0 - \frac{1}{2} (1 + \cos 2\theta_0) \right] \Big\} + \sum_{i'} q_{w_{i'}}$$

$$* \left[-2\theta_1 \bar{\omega}_{w_{i'}}^2 C_{9_{i,i'}} + \theta_1 \sin 2\theta_0 \, C_{68_{i,i'}} - 2\theta_0 \sin \theta_0 \left(C_{65} - C_{69_{i,i}} \right) \right]$$

$$- C_{10_i} (\bar{e}\beta \cos \theta_0 + \bar{g}_{z_5} \cos \theta_0 - \bar{g}_{y_5} \sin \theta_0) - C_{12_i} \left[(\ddot{\beta}^{**} + \beta) \cos \theta_0 \right. \qquad (26)$$

$$\left. + 2\beta \dot{\beta}^{*} \sin \theta_0 \right] + C_{13_i} (\ddot{\beta}^{**} + \beta) \sin \theta_0 - C_{63_i} \left[\ddot{\theta}_0^{**} + \dot{\beta}^{*} (1 - \cos 2\theta_0) \right.$$

$$\left. + \frac{1}{2} \sin 2\theta_0 \right] - \theta_1 \cos 2\theta_0 \left(C_{60_i} - 0.75 \, C_{63_i} \right) - \theta_1 C_{60_i}$$

where i, i' are indices on mode shapes. The C's are constants defined in Ref. 7 which are integral functions of the blade mass distribution, chordwise center of gravity, and flatwise mode shapes and their derivatives. Note that blade lead-lag motion, pushrod effects and damping have been neglected.

Likewise, for each blade the flap angle equation of Ref. 7 can be written, using the same assumptions as the flatwise bending equation.

$$0 = \int_0^{\bar{r}_T} (S_A)_{z_5} \, \bar{r} \, d\bar{r} - \bar{M}_B \, \bar{r}_{cg} \left(\bar{e}\beta + \bar{g}_{z_5} \right) - I_B (\ddot{\beta}^{**} + \beta) - C_{97} (\ddot{\theta}_0^{**} \cos \theta_0$$

where $$- \dot{\theta}_0^{*2} \sin \theta_0 \cdot 2\beta \dot{\theta}_0^{*} \sin \theta_0 - \sin \theta_0) - \bar{e} \sum_i q_{w_i} C_{10_i} \cos \theta_0 \qquad (27)$$

$$\bar{M}_B \, \bar{r}_{cg} = \int_0^{\bar{r}_T} \bar{m} \, \bar{r} \, d\bar{r} \quad ; \quad \bar{I}_B = \int_0^{\bar{r}_T} \bar{m} \, \bar{r}^2 d\bar{r}$$

Equations 26 and 27 define a set of simultaneous equations from which the modal accelerations, $\ddot{q}^{**}_{wi}$, and flapping acceleration, $\ddot{\beta}^{**}$, can be obtained. Straightforward numerical integration will yield the modal and flapping amplitudes so that the aeroelastic flatwise deflections are given by

$$\bar{w}_e = \sum_i q_{w_i}(t,n) \, \gamma_{w_i}(\bar{r}) \qquad (28)$$

and

$$\bar{w}_e' = \sum_i q_{w_i}(t,n) \, \gamma_{w_i}'(\bar{r}) \qquad (29)$$

$$\dot{\bar{w}}_e = \sum_i \dot{q}_{w_i}(t,n) \, \gamma_{w_i}(\bar{r}) \qquad (30)$$

where $\bar{w}'_e$ is the slope of the deflection and $\overset{*}{w}_e$ is the velocity due to aeroelastic motion. n is an index defining the particular blade in question, 1, 2, ... , B.

The implementation of the aeroelastic considerations represents an attempt at close coupling the aeroelastic procedures with the aerodynamic effects. Since the problem is solved sequentially in time, the aeroelastic effects and blade loads must also be determined at each time step. It should be noted that Eqs. 26 and 27 for the modal accelerations and blade flapping acceleration at any instant depend on the current value of the modal amplitudes and flap angles which are not known a priori. A simple technique is considered here. It is assumed the modal quantities, β, $\overset{*}{\beta}$, etc., are known at time t = 0. Based on initial circulations and induced velocities, initial modal accelerations are determined. A simple Euler integration scheme (actually the kinematic relations for velocity and displacement) serve to yield these modal quantities for the next time step. Then, following blade advance and wake deformation, new blade loads are determined giving new modal accelerations and the process is repeated for the next time step.

The blade loads, as developed in Ref. 7 are given by

$$(\bar{S}_A)_{z_5} = \frac{1}{2}\left(\frac{\rho R^2}{m_0}\right)\bar{c}\left(\frac{U}{\Omega R}\right)^2 (C_\ell \cos\phi + C_d \sin\phi) \tag{31}$$

$$(\bar{S}_A)_{y_5} = \frac{1}{2}\left(\frac{\rho R^2}{m_0}\right)\bar{c}\left(\frac{U}{\Omega R}\right)^2 (C_\ell \sin\phi - C_d \cos\phi) \tag{32}$$

These can be converted to conventional distributed loads by multiplying through by $m_0\Omega^2$.

Further Assumptions

Assumptions have been made in order that the computer program be feasible, both economically and practically in terms of required computer storage and run times. Since that part of the analysis which becomes more expensive in both the above categories is the step-by-step analysis of the distorting wake, most of the assumptions made are in this area.

A primary assumption regarding the distorting wake is neglect of the shed vorticity. This amounts to directly neglecting instantaneous increments in the bound circulation and thus the aerodynamic load. The missing increments in bound circulation will also be reflected as missing increments in wake element strength, the effects of which are transmitted to the blades through the wake induced velocity field. Some justification for neglecting shed vortex elements arises from the fact that the circulation strength of the shed vortex elements are normally much lower than the strength of the trailing vortex elements. However, in determining an instantaneous load accurately, as is necessary for determining a high number of loading harmonics, neglecting this shed vorticity is potentially serious. Also, the presence of shed vorticity can alter the shape of the chordwise loading. While this might not be too significant in terms of average loading, it should be important in determining the higher harmonics which are important in terms of the noise signature. Inclusion of shed vorticity should be considered for future refinement of the analysis.

To further simplify the problem, it is assumed that the induced effects are most described by the tip vortices from the individual blades. Hence, the wake distortion is primarily described by the interaction of the various tip vortices. The contribution of the inboard vortex sheet to the tip vortex distorting velocities is assumed constant which implies that the relative positioning of sheet and tip vortex does not change much. This permits the contribution of the inboard sheets to the tip vortex distortions to be computed once, initially, and held constant for all times. Another, perhaps more questionable, assumption is that the tip vortex has no effect on the inboard sheet, although a provision for the sheet to convect under the gust velocity does exist. Essentially what this does is remove the problem from the realm of the full interaction problem, for if the sheet were to deform under the tip vortex, it would also have to be allowed to deform under its own self-induced field which, computationally, is what is being avoided to prevent prohibitive computer time requirements.

The assumption of the wake vortex segments having a core of finite radius with the internal fluid performing a solid body rotation has been discussed in conjunction with the development of Eq. 4. It can be restated

here, however, that such an assumption is necessary to eliminate a singularity in the Biot-Savart law even though the proper determination of this quantity is open to conjecture. The vortex core radius is an input quantity in the analysis.

The aeroelastic phenomena are assumed to be adequately modeled by the rigid body flapping and the first flatwise elastic modes. For the particular case of a transient gust passing over a hovering rotor and wake system, higher modes and coupled effects are most likely negligible. Any errors to higher harmonics of the loading should be less than those provided by neglect of shed vorticity and the lifting line assumption.

Another feature considered to minimize the computational requirements is variable spanwise spacing on the rotor blades depending on the particular item of the solution being considered. The radial segments for determining wake distortions are not necessarily the same as those for determining circulation and inflow. No definite relationship between the number of panels for distortion and the number for circulations have been established; the final distribution selected was based on obtaining a good representation of the tip region. One restriction is that the set of filaments used to compute the distortions is a subset of those used to compute the circulations. The required circulations for the distortions are then simple averages over the number of panels between successive filaments used for the distortion. This amounts to maintaining the same average circulation (or load) between the same filaments in both the distortion solution and the circulation solution.

Sequence of Operations in Computer Program

The preceding analysis was programmed for application on a UNIVAC 1110 digital computer. This consisted of expanding two existing techniques used in UTRC computer programs to perform the necessary computations. The two parent programs are the Circulation Program and the Distorted Wake Geometry Program described by Landgrebe in Refs. 3, 4 & 5.

The Circulation Program computes the circulation distribution over the rotor, given the blade control and response characteristics and a specified wake geometry. In its simplest form, the wake is a classic skewed helicoid in which the trailing vortex filaments are convected relative to the blade by the resultant velocity equal to the vector sum of blade rotational velocity, rotor forward velocity and momentum induced velocity. If wake distortions are important, the basic Circulation Program can be coupled in an iterative procedure with the Distorted Wake Geometry Program. The Distorted Wake Geometry Program is an analytical method whereby, given a bound circulation

distribution, the distortion of the wake filaments can be computed. The basic approach of this method is straightforward and can be sketched as follows: First, an initial wake geometry is assumed and the distribution of circulation along each filament is known from the assumed bound circulation distribution. The classical Biot-Savart law is applied to numerous wake points to determine the induced velocities at these points. These distorting velocities are then numerically integrated over a small time increment by the Euler technique to determine new wake element positions. The process is repeated until the wake points converge to some defined configuration for the given circulation distribution. This wake geometry can then be supplied to the Circulation Program and new circulations computed. If the new values do not agree with the old values within a prescribed tolerance, the new circulations can be supplied to the Distorted Wake Geometry Program to determine a new wake geometry. This wake can then be supplied to the Circulation Program to compute still another set of circulations. This process can be repeated until two successive sets of circulations converge to within a prescribed tolerance.

The previously described method, by virtue of the way in which the wake and circulations are treated, has within it implicit assumptions of steady state or periodic conditions. In general, the transient gust problem is an unsteady, aperiodic phenomenon so that direct application of this procedure cannot model the problem. Thus, for the analysis described herein, the physically more realistic but numerically more difficult procedure was used which consisted of satisfying flow conditions at each point on the blade-wake mesh at each instant of time. Hence, the distorted wake geometry is computed at each time step and the circulations are determined at the individual blade load points at each time step as well. The aeroelastic contributions to the circulation and inflow are also computed at blade load points at each time step. With this fully coupled solution and the creation of new wake points at each time step, the core storage and computation time requirements are increased substantially. Following the determination of the instantaneous blade inflow velocities and the aeroelastic contribution to blade position and velocities, the radial distribution of blade loading is determined at each azimuth position (time step). After the rotor has been allowed to move through its prescribed number of time steps, the blade load distribution is Fourier analyzed in time (azimuth).

This procedure is summarized in the following steps:

Procedure For Time 0 -- Initial Blade Positions

1. Calculate Blade Coordinates.

2. Calculate Wake Coordinates For Starting Hover Condition Based on Input Wake Constants (Prescribed Generalized Wake of Ref. 3).

3. Calculate Or Input Circulations And Induced Velocities.

4. Calculate Blade Response And Airloads.

Procedure For Each Time Step

1. Advance Blades One Azimuth Increment.

2. Add New Trailing Wake Elements.

3. Compute Distorting Velocities And Gust Velocity At Each Tip Vortex Point.

4. Compute Gust Velocity At Each Inboard Wake Point.

5. Compute Wake Geometry.

6. Solve For Circulations At Blades Including Effect Of Gust Velocity And Blade Response.

7. Compute Induced Velocities At Blades.

8. Compute Total Blade Velocity Components Including Gust Velocities.

9. Compute Blade Response And Airloads (Flapping & 1st Bending Mode).

In summary, a numerical method capable of performing an airloads analysis on a hovering rotor subjected to a transient gust has been developed The method computes wake distortion, blade inflow, aeroelastic response and airloads within the restrictions imposed by the assumption described herein.

DISCUSSION OF RESULTS

To perform a demonstration and initial evaluation of the analysis, it was applied to a full-scale rotor test condition. The test rotor is a standard 3-bladed Boeing-Vertol CH-47B rotor with a blade radius of 9.144 m (30 ft), a blade chord of 0.641 m (25.25 in.) and a blade linear twist of -9.12 deg. The test was conducted at the Boeing-Vertol Whirl Tower facility. The selected test condition is defined completely in Ref. 1 (Run 116). The rotor was operated at a nominal thrust of 1.20 mn (27,000 lb) and a tip speed of 228 m/sec (747 fps). The test condition (Run 116) produced blade slap in the presence of an ambient wind speed of 4m/sec (9 mph).

The analysis was run to simulate both an ideal steady hover condition (no ambient wind) and the ambient wind condition. The ideal hover condition was run primarily to (1) check the analysis for convergence by demonstrating that the solutions (wake geometry, blade response and airloads) for hover are time independent, and (2) to evaluate the accuracy of the wake geometry portion of the analysis by comparing the predicted tip vortex geometry with available experimental information obtained from generalized model rotor hover test data. The ambient wind condition was run to (1) predict the tip vortex geometry and airloads for an experimental near hover condition which produced blade slap, (2) check the convergence of the solutions to periodic variations expected for a steady wind condition, and (3) compare the periodic time history of the predicted blade-vortex separation distance with test data. Unfortunately, measured blade airload data was not available for comparison.

Hover Condition

Initial computer runs with the transient airload analysis were made for the hover mode in order to test the fully coupled time step method of solution. The conditions of Run 116 of Ref. 1, without the ambient wind, and a time step increment defined by an azimuth increment of 30 deg were used in the analysis. To start the problem, an initial wake geometry was prescribed using the generalized hovering wake coordinates from Ref. 3 for the appropriate number of blades, twist and thrust level. The intent was to determine whether or not the calculated tip vortex geometry would return to the initially prescribed geometry following a hopefully converged iterative solution of the associated blade and wake circulations, blade response and airloads.

Since the rotor was assumed to be in a steady hover condition, temporal deviations in the bound circulations should not exist in the final solution.

However, in the initial application of the analysis, it was found that unreasonable oscillations in the value of circulation at the three outboard radial stations occurred by the third time step. No tendency was found for these oscillations to diminish as the free wake developed. In investigating the cause of these oscillations, it was found that the airloading in the tip region was very sensitive to the representation of the wake in the tip region. Special attention to the modeling of the wake at the blade tip was thus necessary.

The wake representation, as originally conceived, was assumed to have the trailing vortex segments positioned as straight line segments attached directly to the bound vortex (Fig. 9). An unreasonable magnitude of the contribution of the trailing vortex element attached to the blade tip prompted a reevaluation of this blade-wake representation. The various blade-wake representations considered are shown in Fig. 9 in which $\Gamma(t)$ implies a circulation value at the end of a given time step and $\Gamma(t - \Delta t)$ implies a value at the end of the previous time step. The various vortex models considered represent attempts to improve the modeling of the tip region without going to a complete lifting surface model with shed vorticity. The first permutation on the original model, representation (2) in Fig. 9, was a simple approximation to estimate the effects of chordwise blade geometry. This amounted to assuming the bound vortex to be located at the local one-quarter chord line and modeling the chordwise and trailing vorticity as follows. Vorticity was fixed to the blade in the chordwise direction up to a distance one-quarter chord aft of the trailing edge. At this distance, trailing vortex elements were initiated with strengths determined by the bound circulation gradients at the beginning of the time step. This representation was defined by considerations of numerical lifting surface theory. Although this representation was expected to improve the results, the erratic oscillations of the circulation and induced velocity solutions persisted. Blade-wake representation (3) in Fig. 9 was then used. This representation is similar to representation (2) except that the chordwise vortex elements were omitted.

On the basis of this investigation, representation (3) was selected as the tip model which most reasonably maintained the temporal constancy of bound circulation and produced a reasonably accurate tip vortex geometry for the hover condition. The convergence of the calculated hover wake is shown in Fig. 10. The experimentally determined hovering wake coordinates from Ref. 3 are compared with the predicted coordinates after 41, 62, and 81 time steps corresponding to 1.7, 2.6 and 3.4 blade revolutions, respectively. The convergence of the near wake ($\psi_w < 480$ deg) and the good agreement of the results from the 81st time step with the experimental model data is evident,

particularly in the important region around 120 deg where the following blade is located. The far wake ($\psi_w > 480$ deg) is not converged to a steady geometry. However, this is consistent with the experimental findings reported in Ref. 3 which indicate the tip vortex for a hovering 3-bladed rotor is stable geometrically beyond approximately 480 deg.

It should be mentioned that representation (3) does give an upwash field at the tip which tends to drive the tip into stall. This is due primarily to the reduction of the effect of that part of the self-generated tip filament closest to the bound vortex so that the contribution to the induced velocity field from this filament is more on the order of the tip filament from the first preceding blade. The resulting upwash is then due primarily to the contraction of the tip filament from the preceding blade as it passes near the radial load point.

Hover With Ambient Wind Condition

As mentioned previously, the rotor operating condition from Run 116 of Ref. 1, including the presence of the wind, was selected as the hover with ambient wind condition. The analysis was started using the same prescribed experimental wake geometry as the previous case for the hover without wind condition. The 4 m/sec (9 mph) ambient wind measured for Run 116 was applied over the entire rotor at the first time step as an impulsive gust from the 225 deg ("northwest" in Ref. 1) azimuth direction. In order to simulate analytically the imposed steady wind condition, the rotor was subjected to the gust representation described by Eq. 5 with $v_{gz} = 0$. The results of applying the analysis to this condition are summarized in Figs. 11 through 14.

Initially calculated time histories of blade airloading (thrust loading*) at selected radial stations, 0.80 R, 0.87 R, 0.939 R and 0.985 R, are presented in Fig. 11. In this figure, the blade azimuth angle is representative of time; i.e., each 15 deg of blade travel represents a time step in the computer analysis. The analysis was run for 74 time steps which resulted in 1110 deg of azimuth travel for each blade which is slightly more than three revolutions. As shown in Fig. 11, the predicted blade transient loading tends to diminish after about two revolutions of blade travel at all radial stations. The maximum values attained at 0.939 R as well as the high, nearly constant, values at 0.985 R are due to

---

*Blade thrust loading is presented in metric units, N/cm. To convert to English units, lb/in, multiply by 11.3.

these stations reaching their stall limit under the influence of the upwash induced primarily by the tip vortex of the preceding blade. Although experimental airloads were not available for comparison, these initial results tended to be as anticipated in that they show an initial transient response followed by a tendency to settle to a periodic, one-per-rev variation. A periodic distribution, similar for each blade, is realistic for this condition where the ambient wind, initially applied as an impulsive gust velocity, is continued in time as a steady wind. However, the solution was questioned, due to the high harmonics ("spikes") in the thrust loading (e.g., at 0.872 R near ψ = 700 deg for blade 3 and at 0.939 R near 780 deg and 1130 deg for blade 2). These spikes were found to be caused by numerical rather than physical means, and were due to an inconsistency in the vortex model. This inconsistency occurred because of the attempt to model the inflow at the 9 radial stations and interpolate to 15 radial stations to compute the blade loads. Since the 9 radial positions at which the inflow is computed are not a subset of the 15 positions at which the blade loads are computed, the interpolation scheme to compute the inflow at the load points, given the inflow points, can lead to completely erroneous results. These spikes were traced to this inconsistency and so must be discounted as a possible noise source.

The case was recomputed with the aerodynamic load stations selected to coincide with the 9 induced velocity stations to provide a consistent model. Airload data at four outboard blade stations (0.75 R, 0.85 R, 0.925 R and 0.99 R) for 3 revolutions are presented in Fig. 12. Similar to the previous results, the blade loads very quickly settle into a one-per-rev periodic fluctuation compatible with a steady forward flight response. The in-plane loads, presented in Fig. 13, show very little unsteady response.

Comparing Figs. 11 and 12, most of the numerical transients have been eliminated by requiring the aerodynamic load points and inflow stations to be coincident. It can be noted that the small spike near ψ = 500 deg in Fig. 12 is due to a near vortex passage, and may be considered a transient nonrecurring effect for this steady wind condition. These results show that in modeling the time histories of rotor airloads by a transient analysis with a deforming wake that it is necessary for airload and inflow stations to be coincident. Even though the comparison does demonstrate the sensitivity of the results to the model selected, it must be emphasized that inferences from combining the two sets of data must be made with care. The sets of airload stations are different, and the 9-station set is not a subset of the 15 original stations.

It is recognized that the selected steady rotor operating condition does not represent a true transient gust case. A transient gust implies a time-wise variation in wind over a rotor-wake system in equilibrium. What has actually been investigated is the condition of a uniform in-plane wind applied impulsively over a rotor-wake system which is not initially in equilibrium. As a result, the transients noted are not realistic, but are numerical due to this nonequilibrium. In future applications, when a true gust condition is to be investigated, the procedure should be to run the analysis in the steady condition (without the gust) for a sufficient number of time steps to achieve equilibrium of the solutuon, and then the gust velocities should be applied. This should eliminate numerical transients in the predicted transient air-loads produced by the gust.

Due to the limitations in the available experimental data for correla-tion purposes, the achievement of the one-per-rev periodicity and the real-istic wake results predicted for the hover (no wind) condition have been the major items presented to this point which indicate some physical validity of the new analysis. Other than acoustic data, the one parameter for which use-ful test data is available in Ref. 1 is the time history of the blade-vortex separation distance. This is the vertical distance between a blade and the tip vortex from the preceding blade as shown in Fig. 14, and was measured using a rotating camera mounted at the hub of the CH-47B rotor. Considering the limited extent of the whirlstand data and the measured accuracy of the wind conditions, good agreement is shown in Fig. 14 between the analytical results and the test data. The analytical separation results exhibit a one-per-rev sinusoidal variation with blade azimuth similar to that indicated by a composite of test data form several runs in Ref. 1. The repeatability of the analytical results for blades 1, 2, and 3 is consistent with the repeat-ability of the test data for two (2) rotor cycles which is indicative of a steady wind condition. The differences in amplitude and phase angle relative to the upwind direction are presumed to be at least partially attributable to the inaccuracies in the measurements of wind velocity and direction. The wind measurements were made on a tower 2.5 diameters (4.57 m, 150 ft) away from the rotor center, and the wind direction was recorded only generally as northwest for this condition rather than as a specific azimuth in the fixed reference system (such as the 225 deg used in the analysis). These results, coupled with the correlation demonstrated in Fig. 10 for the hover condition, provide an encouraging indication of the capability of the analysis to pre-dict reasonably accurate tip vortex geometries.

CONCLUDING REMARKS AND RECOMMENDATIONS

The development of the transient wake and airload analysis has resulted in a computer program in which the solution for the hovering rotor wake, inflow, aeroelastic response and airloads are solved in a coupled manner at sequential time steps, with or without the influence of an imposed gust.

Based on the initial applications of the analysis, reported herein, the predicted tip vortex coordinates are in reasonable agreement with the limited experimental data. Unfortunately airload data was not available for comparison, so that only the achievement of the periodic behavior of the airload solutions for a steady ambient wind condition could be used to indicate some degree of physical validity of the analysis.

Although the above results are somewhat encouraging, the requirement for refinements to the analysis is evident. These refinements should be incorporated before the analysis is applied to determine airloadings for the impulsive noise problem. Recommendations regarding these refinements are presented below:

1. Due to computer time and storage limitations, application of the analysis using sufficiently small azimuth increments (e.g., 3 deg) to determine the high harmonics of blade loading required for impulsive noise prediction is currently prohibitive. (The use of 15 deg increments for the ambient wind condition required approximately 3 hours of UNIVAC 1110 computer time.) A significant reduction in computer time and storage requirements could be achieved through selective vortex element interactions in the tip vortex geometry calculations such as described in Ref. 5. Also, the feasibility of acquiring higher harmonics of airloading without a general azimuth increment decrease should be explored. This might be achieved through locally decreasing the azimuth increment when a tip vortex is in close proximity to a blade, or through a decrease in the azimuth increment for the loading solution relative to that used for the wake representation.

2. In order to further reduce computer time and program complexity, a sensitivity study should be performed to determine the cost effectiveness of several items, both input and internal to the computer program. For example, the sensitivity of the results to the input number of wake revolutions should be investigated to determine the proper compromise between accuracy and computer cost. Also, although the first flatwise bending mode deflections contribute to the blade-vortex spacing, it is recognized that for many rotors the added complexity of including this aeroelastic blade response may be unwarranted.

3. The blade/wake representation should be refined in that it appears that the lifting line representation used may be insufficient for providing essential flow details at the blade tip. The sensitivity of the inflow at the tip to the vortex representation in the immediate vicinity of the blade should be investigated further. The influence of including a representation for shed vorticity and the sensitivity to time step size and stall limit should be included in the investigation. Regarding the requirement for a lifting surface representation of the blade, a better understanding of the fundamental nature of impulsive noise would be helpful. That is, if it were known that impulsive noise can be determined from chordwise averaged airloads, then lifting line assumptions may be sufficient. However, if it is dependent on local conditions on the blade, such as the occurrence of local pressure fluctuations or local sonic conditions, compressible lifting surface theory is required.

4. Additional cases should be run to continue evaluation of the computer analysis. In particular, the analysis should be correlated with a test configuration for which a consistent set of wake geometry and airload data is acquired. Also, the analysis should be applied to transient gust conditions, to determine if transient blade-vortex intersections and associated impulsive type airloads are predicted which could be conducive to blade slap.

REFERENCES

1. Sternfeld, H.; Spencer, R. H.; and Schairer, J. O.: An Investigation of Noise Generation on a Hovering Rotor (Part I). The Boeing Company, Vertol Division, Report No. D210-10229-1, Prepared for the U. S. Army Research Office - Durham, January 1971.

2. Sternfeld, H.; Bobo, C.; Carmichael, D.; Fukushima, T.; and Spencer, R: An Investigation of Noise Generation on a Hovering Rotor (Part II). The Boeing Company, Vertol Division, Report No. D210-10550-1, Prepared for the U. S. Army Research Office - Durham, November 1972.

3. Landgrebe, A. J.: An Analytical and Experimental Investigation of Helicopter Rotor Hover Performance and Wake Geometry Characteristics. United Aircraft Research Laboratories, USAAMRDL Technical Report 71-24, Prepared for the Eustis Directorate, U. S. Army Air Mobility Research and Development Laboratory, June 1971, AD728835. (Summarized in --

   Landgrebe, A. J.: The Wake Geometry of a Hovering Helicopter Rotor and Its Influence on Hover Performance. Journal of the American Helicopter Society, vol. 17, no. 4, October 1972).

4. Landgrebe, A. J.; and Egolf, T. A.: Rotorcraft Wake Analysis for the Prediction of Induced Velocities. United Technologies Research Center, USAAMRDL-TR-75-45, Prepared for the Eustis Directorate, U. S. Army Air Mobility Research and Development Laboratory, 1975.

5. Landgrebe, A. J.: An Analytical Method for Predicting Rotor Wake Geometry. Journal of the American Helicopter Society, vol. 14, no. 4, October 1969.

6. Hall, G. F.: Unsteady Vortex Lattice Techniques Applied to Wake Formation and the Statically Thrusting Propeller. NASA CR-132686, 1975.

7. Arcidiacono, P. J.: Prediction of Rotor Instability at High Forward Speeds, Volume I - Steady Flight Differential Equations of Motion for a Flexible Helicopter Blade with Chordwise Mass Unbalance. United Aircraft Research Laboratories, USAAVLABS Technical Report 68-18A, Prepared for the U. S. Army Aviation Materiel Laboratories, February 1969, AD685860.

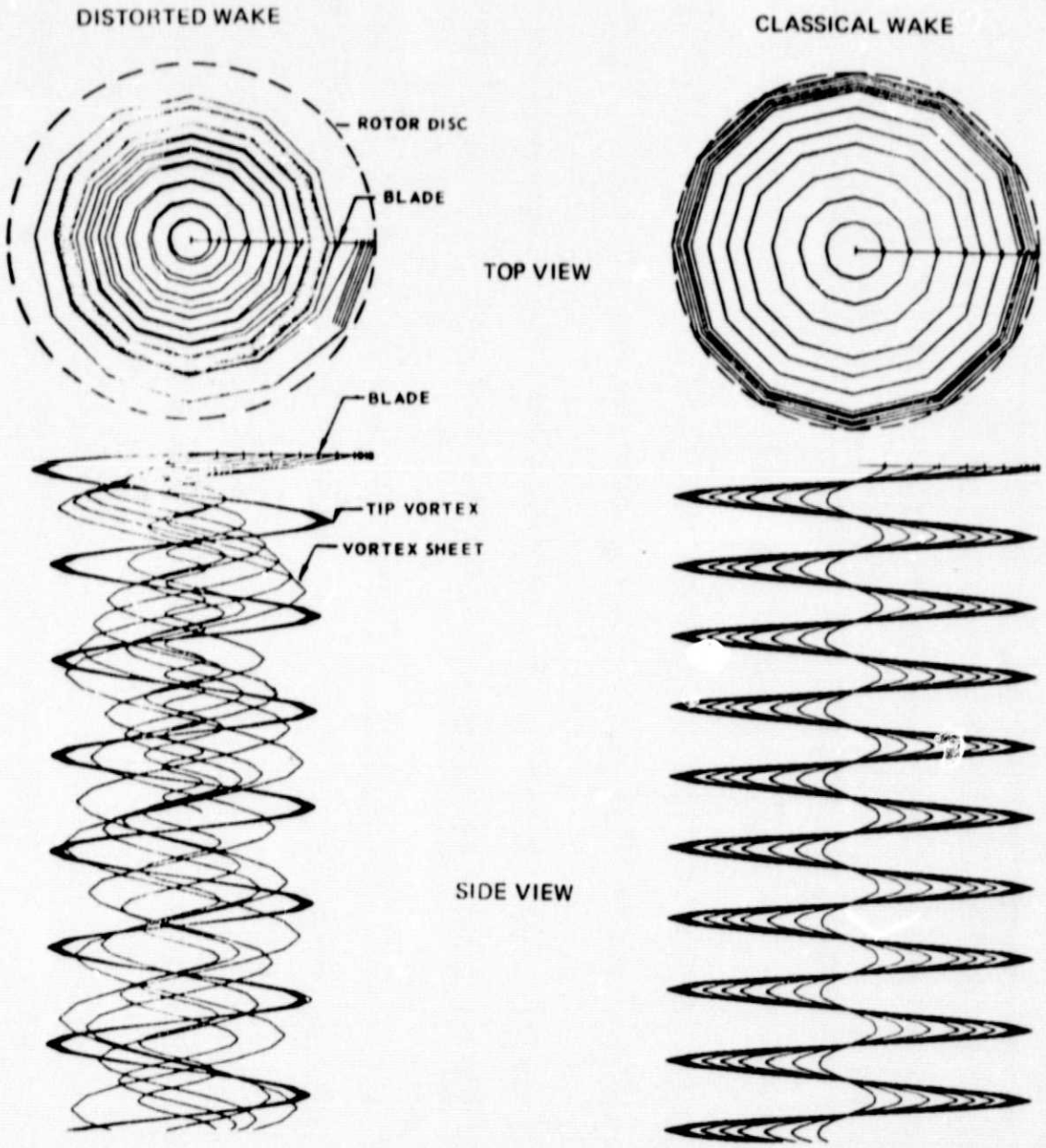

Figure 1. Computer Wake Representations for One Blade of A Hovering Rotor -- Classical and Distorted Wake Models.

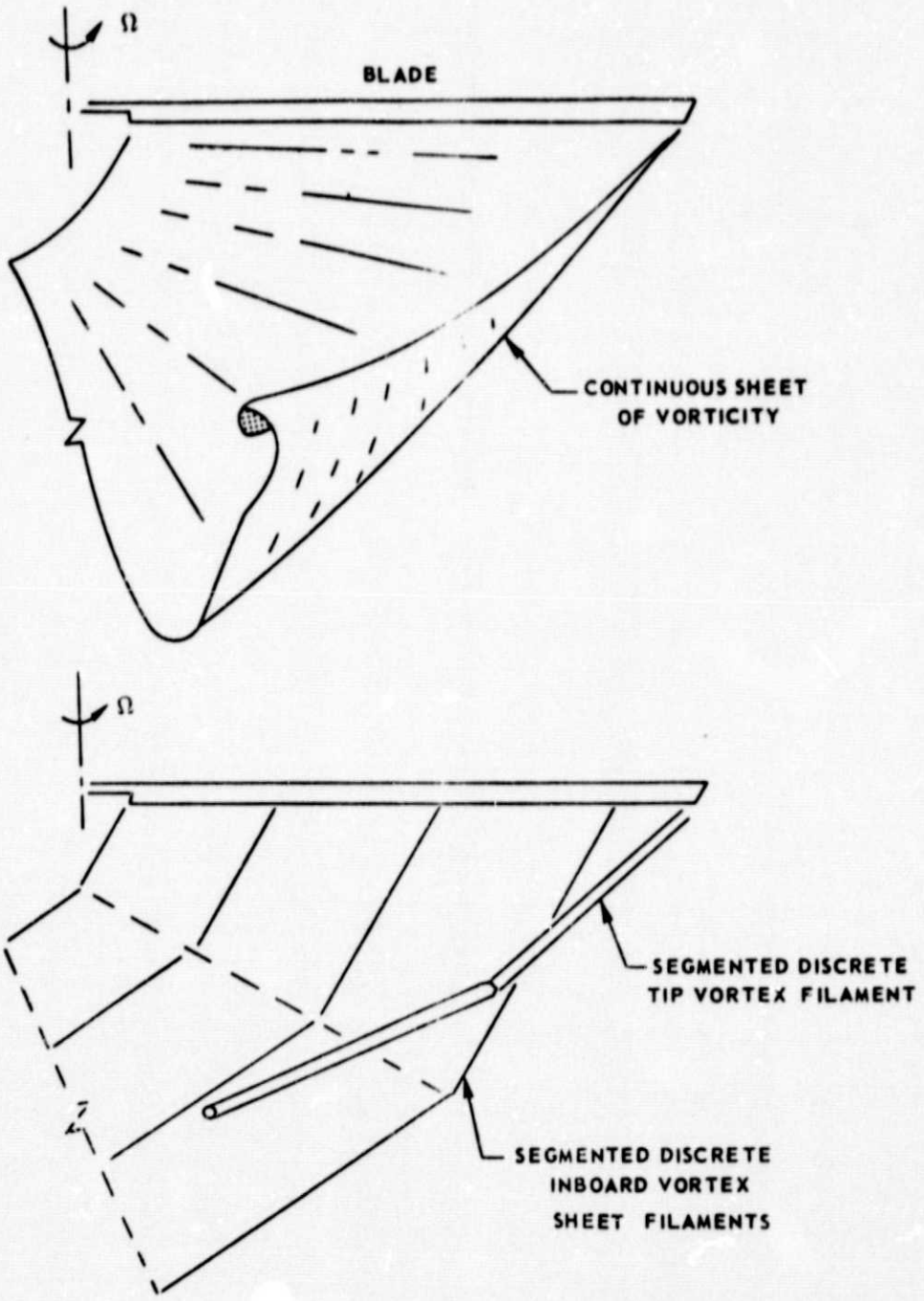

Figure 2. Segmented Discrete Vortex Representation of the Wake.

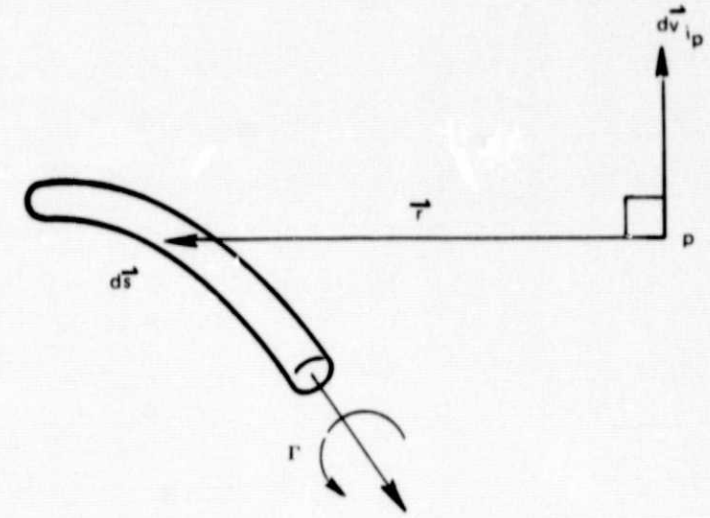

a) DIFFERENTIAL SEGMENT

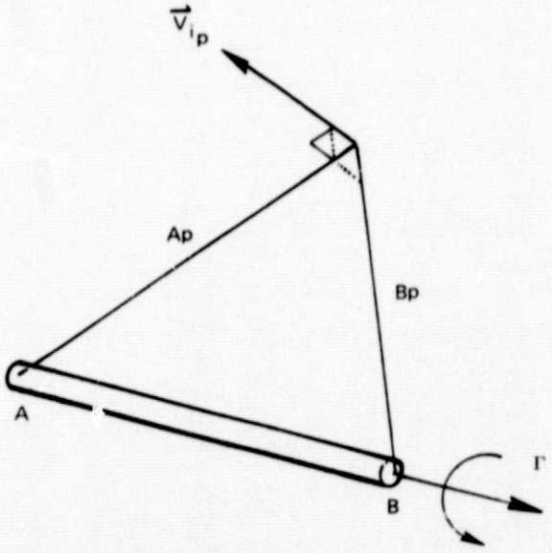

b) STRAIGHT LINE SEGMENT

Figure 3. Geometry for Velocity Induced by a Vortex Segment.

R09-35-1

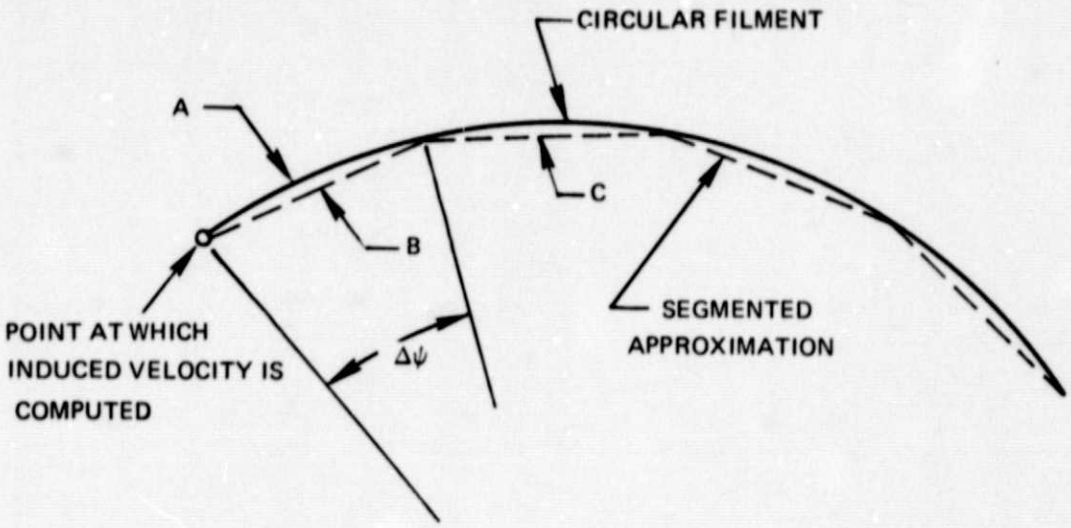

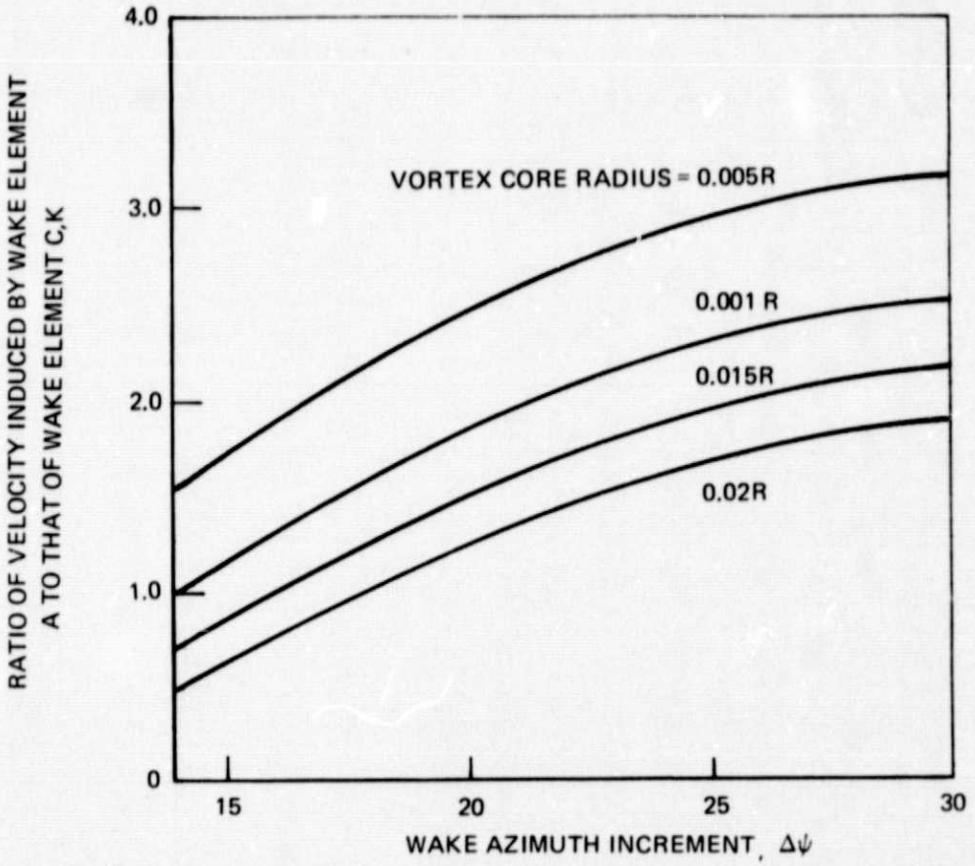

Figure 4. Scaling Factor to Approximate the Induced Velocity Contribution of an Adjacent Curved Vortex Segment.

R09-35-2

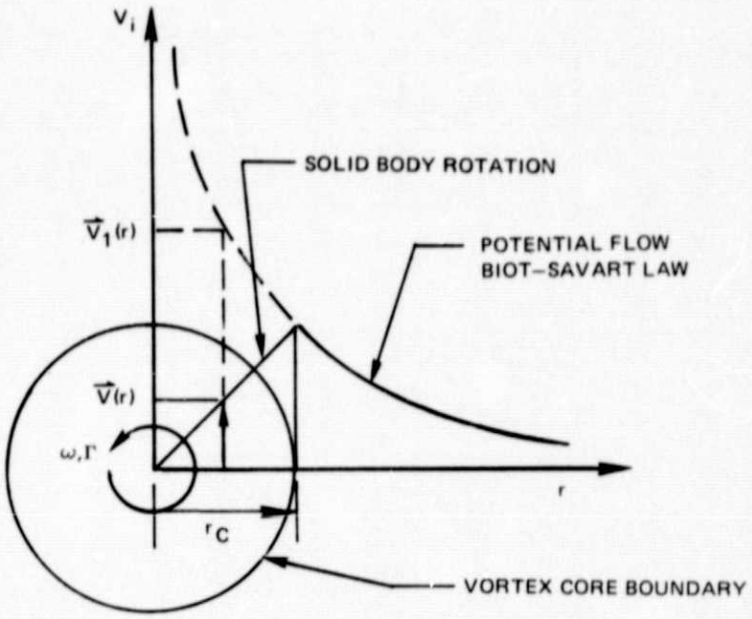

a) END VIEW

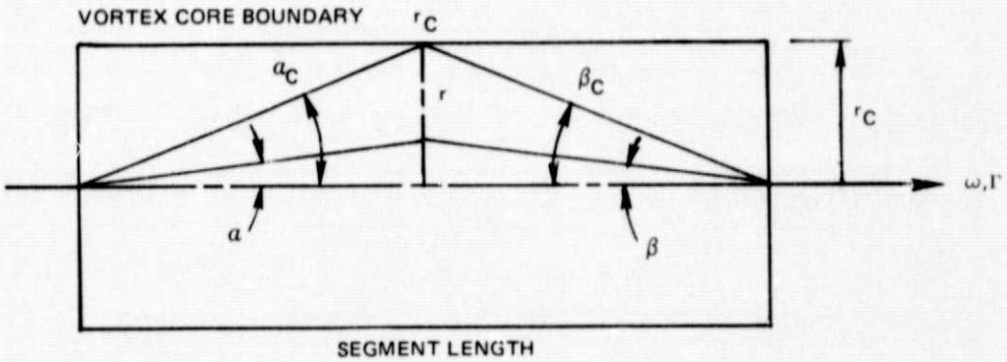

b) SIDE VIEW

Figure 5. Vortex Segment Geometry for Computing Velocities Within the Vortex Core.

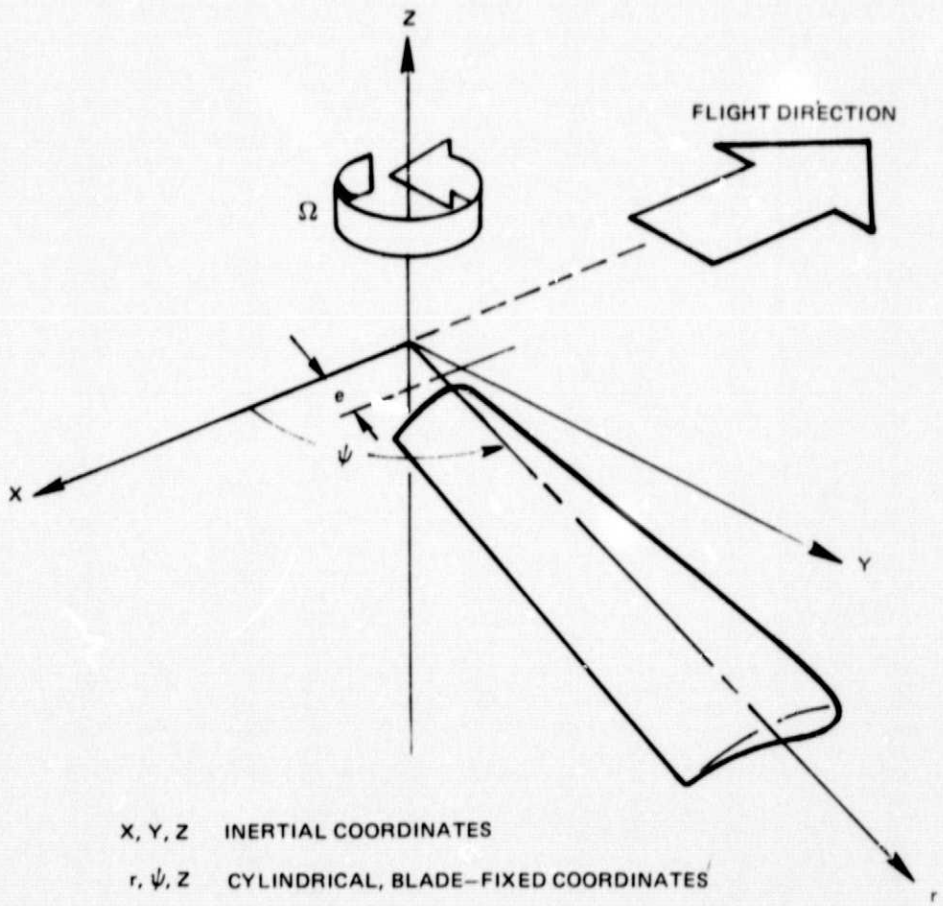

X, Y, Z INERTIAL COORDINATES

r, ψ, Z CYLINDRICAL, BLADE–FIXED COORDINATES

e HINGE OFF–SET

Figure 6. Coordinate System.

R09–35–4

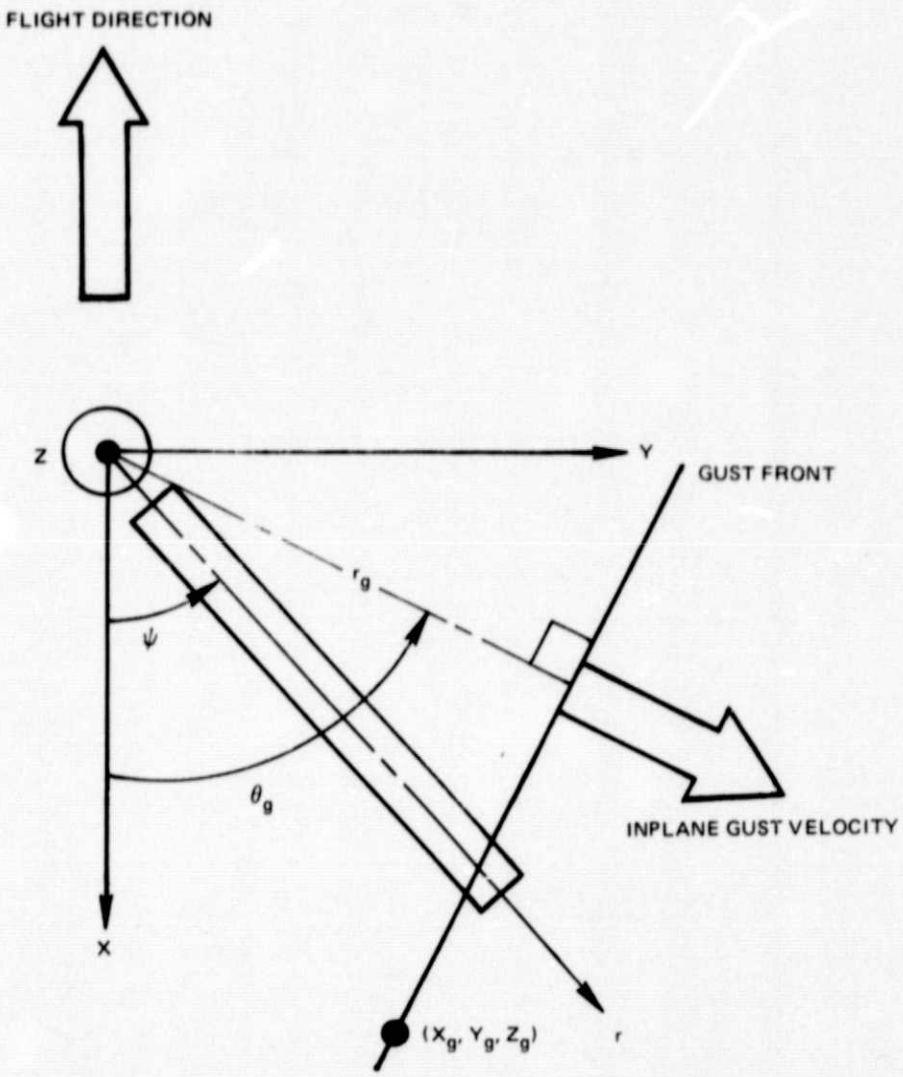

X, Y, Z	INERTIAL COORDINATES
r, ψ, Z	CYLINDRICAL BLADE-FIXED COORDINATES
X_g, Y_g, Z_g	POINT ON GUST FRONT
r_g, θ_g	GUST FRONT COORDINATES

Figure 7. Gust Coordinates.

R09-35-5

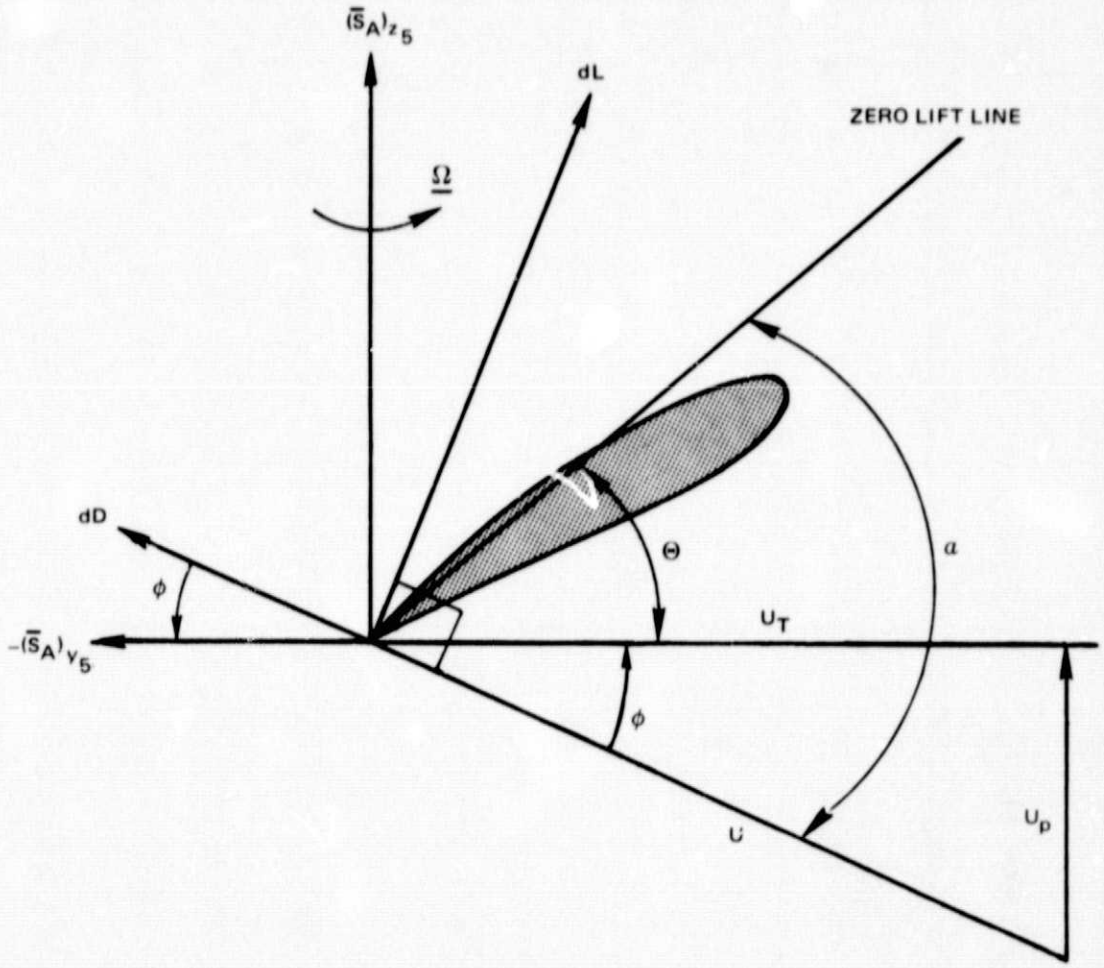

Figure 8. Blade Element Forces and Velocities.

R09-35-6

BLADE–WAKE REPRESENTATION

REMARKS

1.) BOUND VORTEX

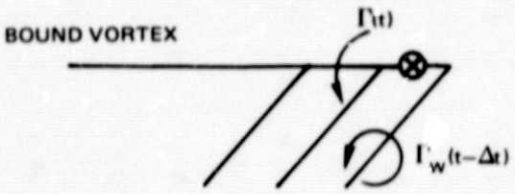

TRAILING VORTICES

ORIGINALLY CONCEIVED MODEL FOR TRANSIENT WAKE. VERY LARGE FLUCTUATIONS IN BOUND Γ AT TIP. LARGE FLUCTUATIONS IN INDUCED VELOCITY AT TIP.

TIME STEP 1	$v_i \otimes$ = −26.4 m/s
TIME STEP 2	$v_i \otimes$ = −33.8 m/s
TIME STEP 3	$v_i \otimes$ = +7.2 m/s

2.) BOUND VORTEX
BLADE C/4

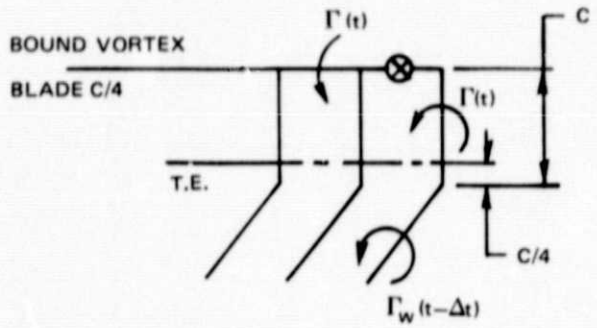

BOUND VORTEX AT C/4; TRAILING ELEMENTS LEAVE FROM C/4 DOWNSTREAM OF T.E.; CHORDWISE ELEMENTS INCLUDED. VERY ERRATIC RADIAL Γ AND v_i DISTRIBUTION.

3.) BOUND VORTEX
BLADE C/4

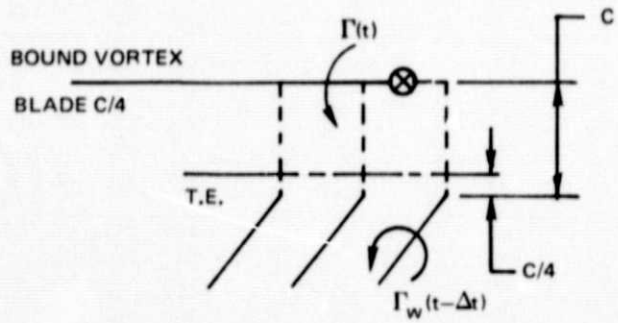

SAME AS MODEL 2 EXCEPT CHORDWISE ELEMENTS OMITTED. MAINTAINS SHAPE OF DISTRIBUTION OF CIRCULATION IN HOVER. UPWASH FIELD AT TIP REGION NOTED.

TIME STEP 1	$v_i \otimes$ = 1.2 m/s
TIME STEP 2	$v_i \otimes$ = 0.9 m/s
TIME STEP 3	$v_i \otimes$ = 1.5 m/s

Figure 9. Blade-Wake Vortex Segment Representations.

R09–35–7

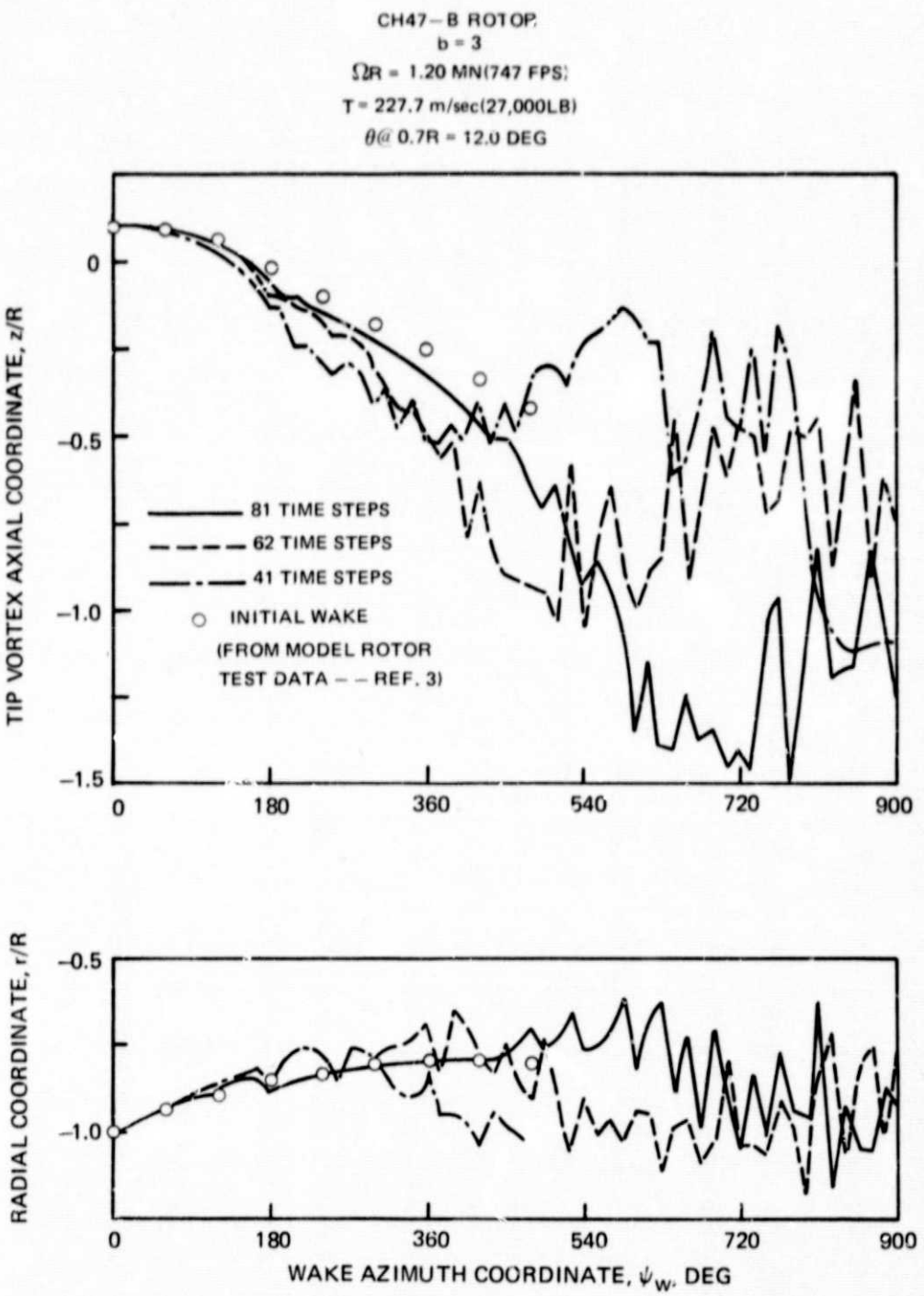

Figure 10. Convergence of the Tip Vortex Geometry for a Hover Without Wind Condition and Comparison With Model Rotor Test Data.

R08–131–2

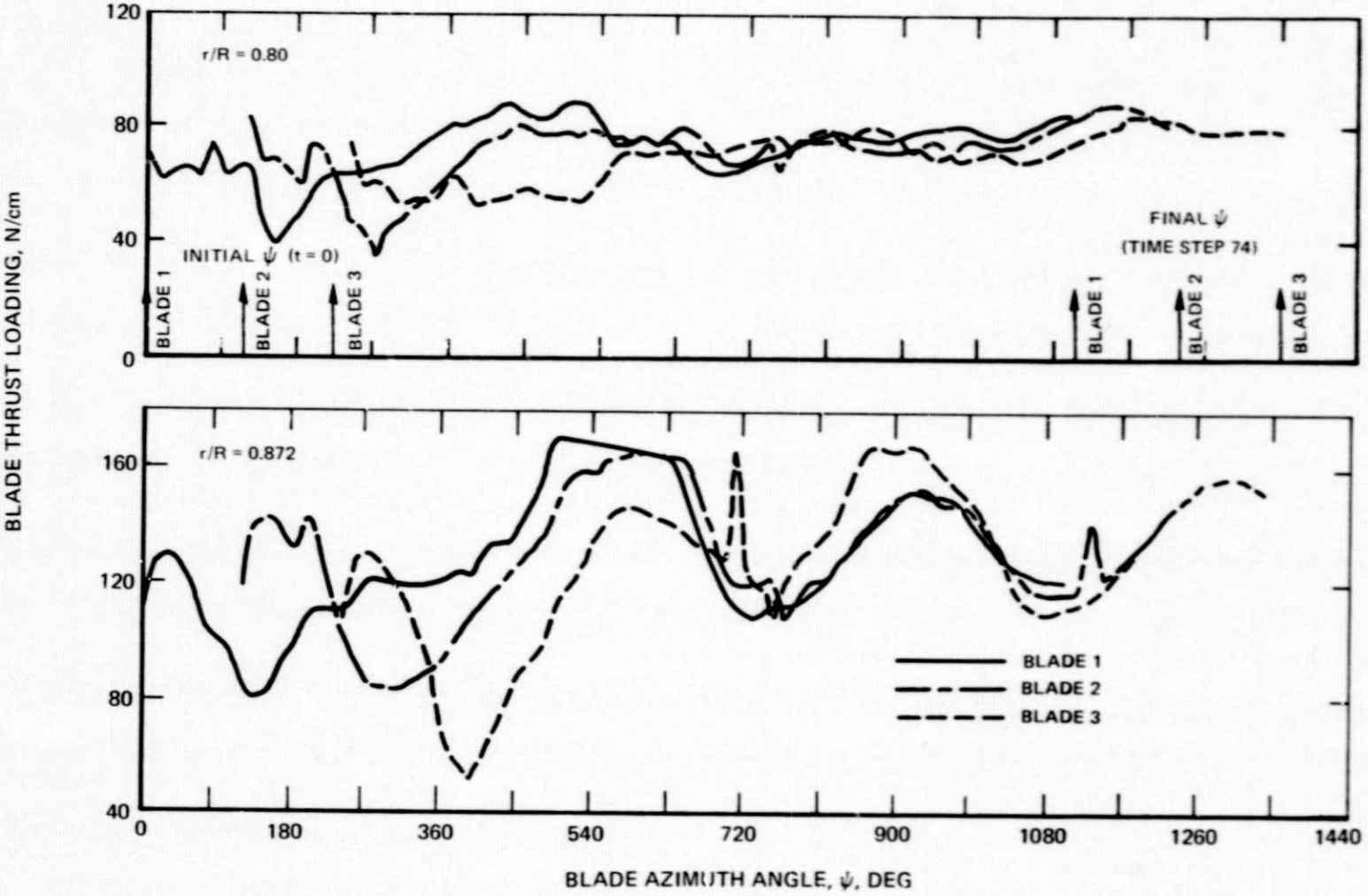

(a) 0.8R and 0.872 Blade Stations

Figure 11. Initial Calculations of Time Histories of Blade Airloading for the Hovering Rotor With a Steady Ambient Wind Imposed During the First Time Step.

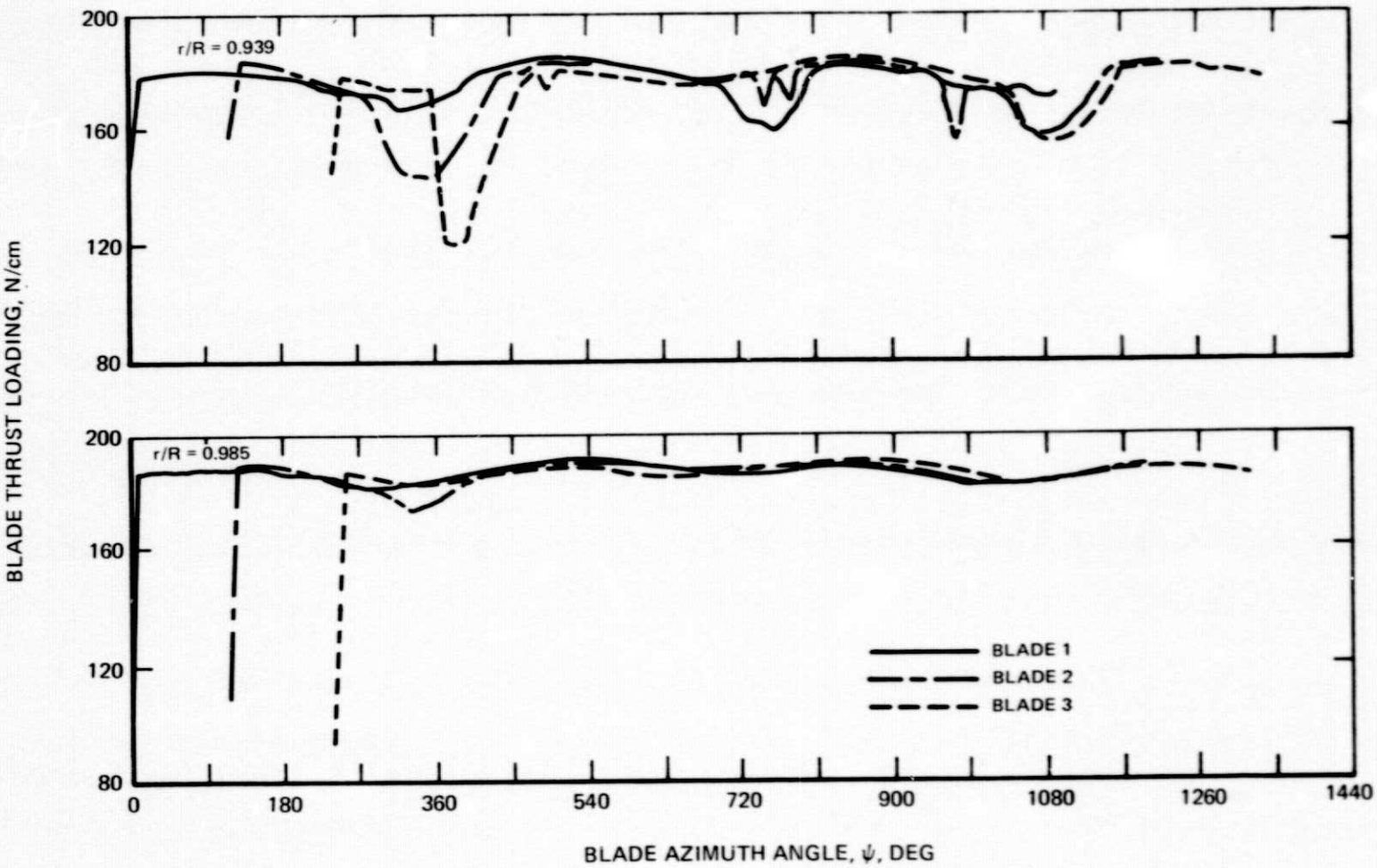

(b) 0.939R and 0.985 Blade Stations

Figure 11. Concluded.

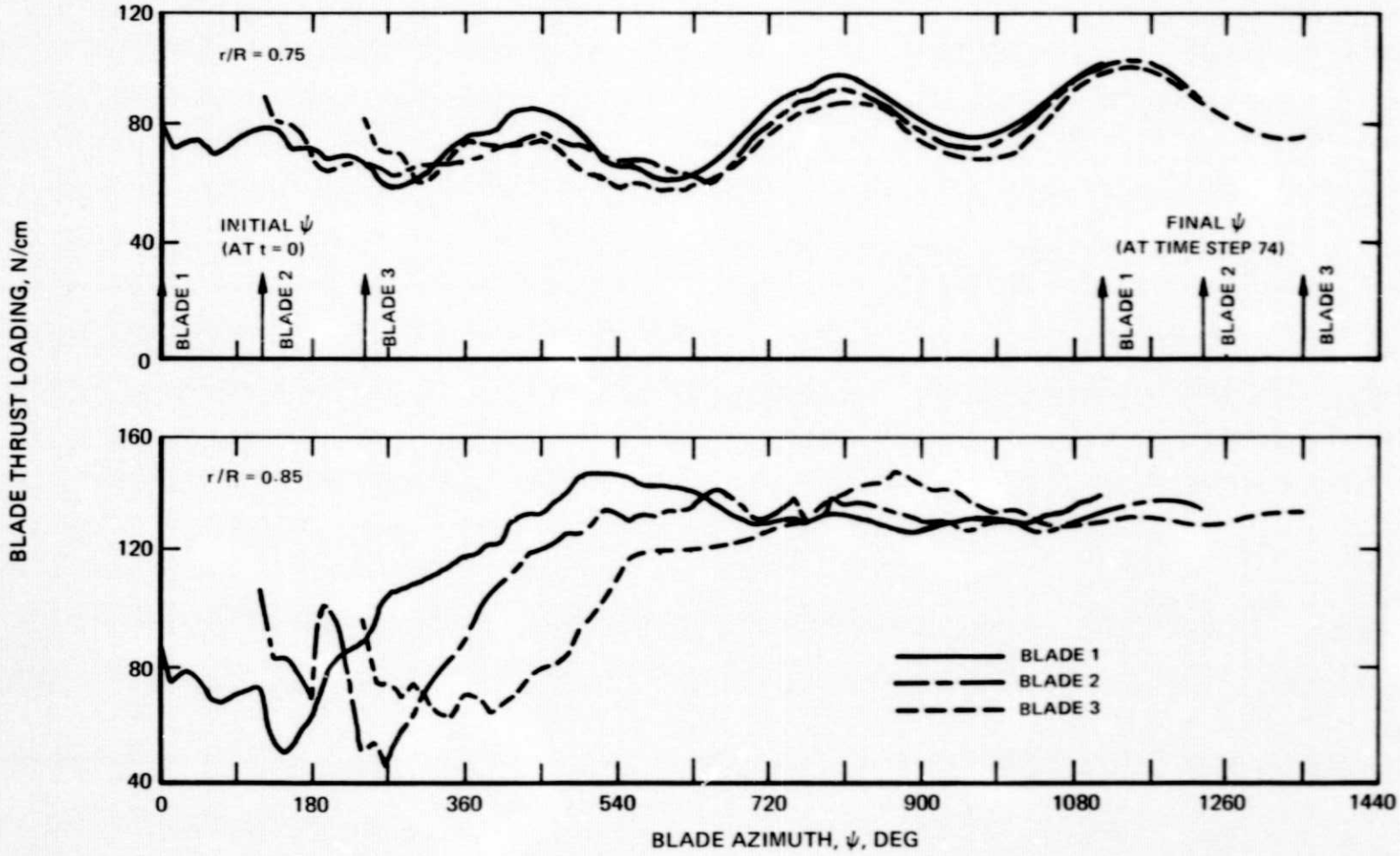

(a) 0.75R and 0.85R Blade Stations.

Figure 12. Final Calculations of Time Histories of Blade Airloading for the Hovering Rotor With a Steady Ambient Wind Imposed at the First Time Step.

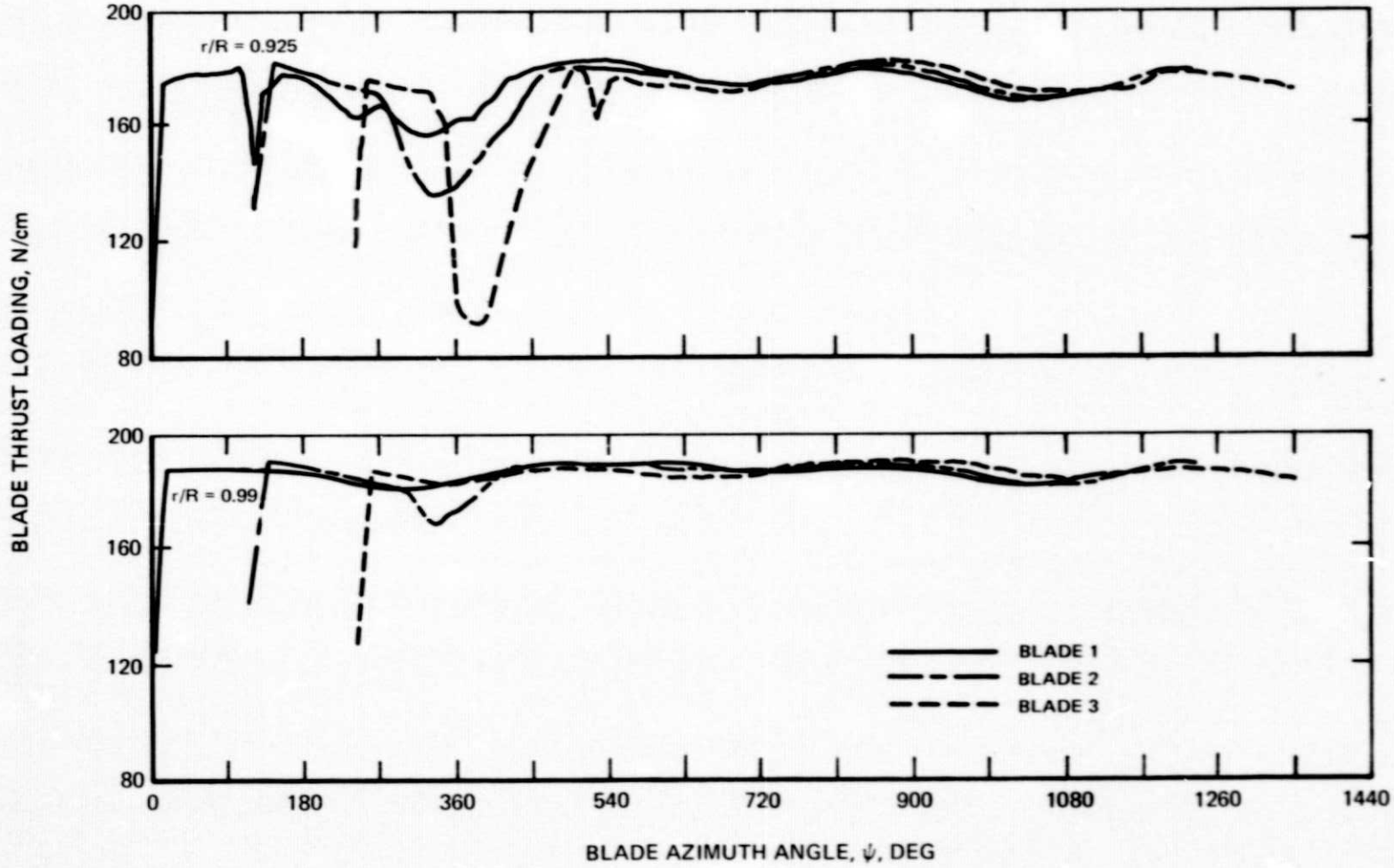

(b) 0.925R and 0.99R Blade Stations.

Figure 12. Concluded.

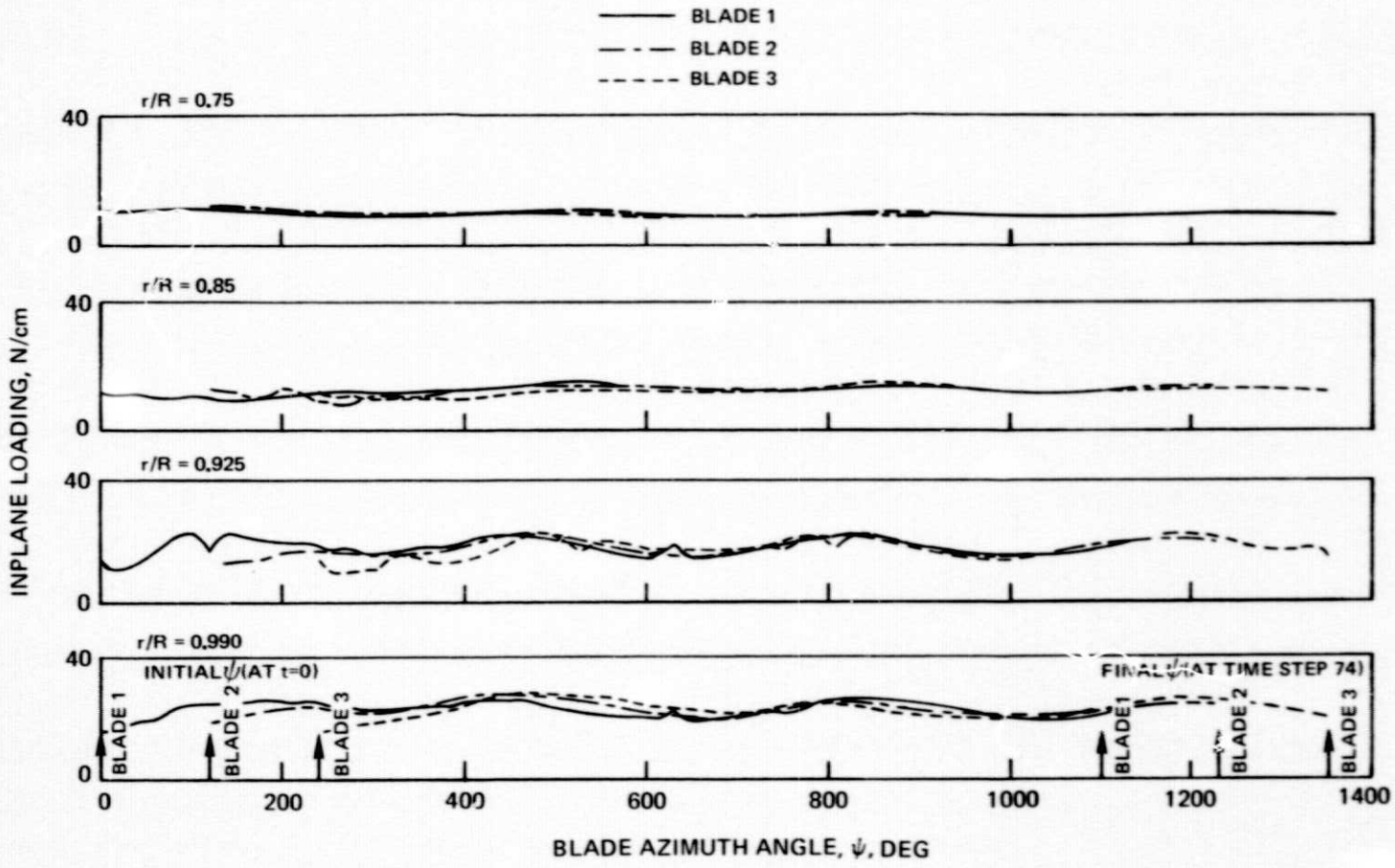

Figure 13. Time Histories of Blade Inplane Loading for the Hovering Rotor With a Steady Ambient Wind Imposed at the First Time Step.

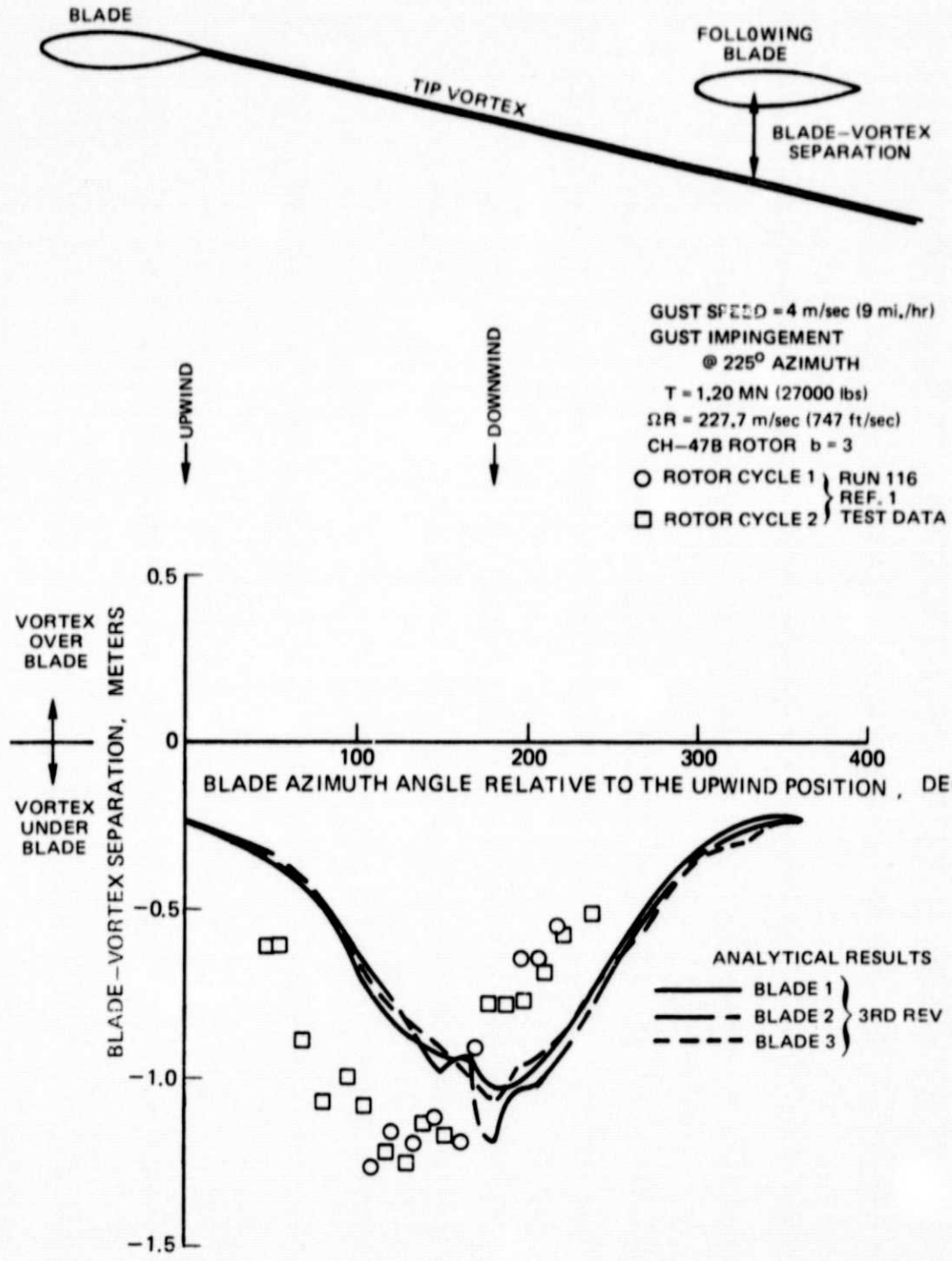

Figure 14. Comparison of Predicted and Measured Blade-Tip Vortex Separation Distances for the Hovering Rotor With a Steady Ambient Wind.

R08–131–1